forests

MDPI

Article

Estimating and Modeling *Pinus contorta* Transpiration in a Montane Meadow Using Sap-Flow Measurements

Simon Marks *,†, Christopher Surfleet and Bwalya Malama

Natural Resources Management and Environmental Science Department, California Polytechnic State University San Luis Obispo, 1 Grand Avenue, San Luis Obispo, CA 93407, USA; csurflee@calpoly.edu (C.S.); bmalama@calpoly.edu (B.M.)

* Correspondence: simonmarks36@gmail.com

† This manuscript is part of a Master's Thesis by the first author. Available online: https://digitalcommons.calpoly.edu/theses/2396/ (accessed on 8 October 2024).

Abstract: This study quantifies the transpiration of encroached lodgepole pine (*Pinus contorta var. murryana* (Grev. & Balf.) Engelm.) in a montane meadow using pre-restoration sap-flow measurements. Lodgepole pine transpiration and its response to environmental variables were examined in Rock Creek Meadow (RCM), Southern Cascade Range, CA, USA. Sap-flow data from lodgepole pines were scaled to the meadow using tree survey data and then validated with MODIS evapotranspiration estimates for the 2019 and 2020 growing seasons. A modified Jarvis–Stewart model calibrated to 2020 sap-flow data analyzed lodgepole pine transpiration's correlation with solar radiation, air temperature, vapor pressure deficit, and soil volumetric water content. Model validation utilized 2021 growing season sap-flow data. Calibration and validation employed a Markov Chain Monte Carlo (MCMC) approach through the DREAM$_{(ZS)}$ algorithm with a generalized likelihood (GL) function, enabling parameter and total uncertainty assessment. The model's scaling was compared with simple scaling estimates. Average lodgepole pine transpiration at RCM ranged between 220.6 ± 25.3 and 393.4 ± 45.7 mm for the campaign (mid-July 2019 to mid-August 2020) and 100.2 ± 11.5 to 178.8 ± 20.7 mm for the 2020 partial growing season (April to mid-August), akin to MODIS ET. The model aligned well with observed normalized sap-velocity during the 2020 growing season (RMSE = 0.087). However, sap-velocity, on average, was underpredicted by the model (PBIAS = −6.579%). Model validation mirrored calibration in performance metrics (RMSE = 0.1233; PBIAS = −2.873%). The 95% total predictive uncertainty confidence intervals generated by GL-DREAM$_{(ZS)}$ enveloped close to the theoretically expected 95% of total observations for the calibration (94.5%) and validation (81.8%) periods. The performance of the GL-DREAM$_{(ZS)}$ approach and uncertainty assessment in this study shows promise for future MJS model applications, and the model-derived 2020 transpiration estimates highlight the MJS model utility for scaling sap-flow measurements from individual trees to stands of trees.

Keywords: heat pulse velocity sap-flow; evapotranspiration; meadow encroachment; Markov Chain Monte Carlo; DiffeRential evolution adaptive metropolis (DREAM) algorithm

Citation: Marks, S.; Surfleet, C.; Malama, B. Estimating and Modeling *Pinus contorta* Transpiration in a Montane Meadow Using Sap-Flow Measurements. *Forests* **2024**, *15*, 1786. https://doi.org/10.3390/f15101786

Academic Editor: Changliang Shao

Received: 6 September 2024
Revised: 1 October 2024
Accepted: 7 October 2024
Published: 11 October 2024

1. Introduction

Montane meadows comprise a small proportion of the montane landscape, but their hydrologic and ecologic functions make them indispensable environmental features. Meadows promote biodiversity in forest ecosystems and enhance water storage in upper watersheds [1]. Meadows in the Sierra Nevada and Cascade Ranges face a myriad of threats, including overgrazing, habitat degradation associated with recreation, fire prevention/regime alteration, residential/commercial development, and habitat fluctuations tied to climate change [2]. Meadow degradation typically results in drier soils with less organic matter, lowered water tables, and changes in vegetation species [1,3]. Drier soil provides the opportunity for conifer encroachment, which refers to the replacement of meadow vegetation

by conifer forest [2,4–7]. The past and ongoing decline of meadows due to conifer encroachment suggests the implementation of restoration techniques to remove the encroached conifers [2,8–10].

An approach for restoring meadow habitat with conifer encroachment is to remove the conifers, which has been shown to increase seasonal soil moisture and groundwater levels by reducing water losses from interception and transpiration (ET) [10–12]. This change in the meadow water balance is envisioned to facilitate the recovery of meadow vegetation species generally controlled by soil water, encouraging biodiversity [2,9,13]. Conifer transpiration represents a component of the pre-restoration water budget, suggesting the importance of understanding its effect on meadow habitat.

A direct quantification of conifer transpiration enables the partitioning of ET in a meadow water budget for the discovery of hydrologic change in meadow functions. A study, 4 years following the removal of lodgepole pine (*Pinus contorta var. murryana* (Grev. & Balf.) Engelm.), demonstrated an increase in soil moisture but no decrease in summer and fall soil moisture, suggesting relatively similar transpiration from newly established meadow vegetation during the summer growing season compared to the lodgepole pine [10]. However, the loss of intercepted precipitation from the tree canopy increased soil moisture in the meadow during the wet season and the beginning of summer, when herbaceous meadow vegetation emerges. In other studies, meadows degraded by woody vegetation (not conifers) had lower ET rates relative to their meadows with herbaceous vegetation, further substantiating the improvement in hydrologic functions necessary in meadow recovery [14,15].

Climate and energy variables of air temperature, solar radiation, and vapor pressure deficit exert controls on conifer transpiration [16–18]. Like soil moisture control, our knowledge of climatic and energy drivers of meadow conifer transpiration is insufficient due to increasing temperatures and climatic variability. Montane meadows in the Sierra Nevada and Southern Cascades are considered highly vulnerable to a changing climate due to a shift toward greater rain precipitation inputs. This results in an increase in winter runoff, compared to snow precipitation, decreasing soil moisture and groundwater during spring and summer, the period of herbaceous vegetation emergence and growth [19,20].

This work presents results from heat-pulse sap-flow measurements of lodgepole pine (*Pinus contorta var. murryana* (Grev. & Balf.) Engelm.) in a montane meadow prior to its restoration by tree removal at Rock Creek Meadow (RCM). The goal of the work was to estimate lodgepole pine transpiration in RCM for an approximately 1-year period and to investigate environmental drivers of lodgepole pine transpiration during the growing season. The research objectives for these pre-restoration results were: (1) Scale sap-flow tree data to the meadow's lodgepole pine transpiration and compare the transpiration estimates to remote sensing-based moderate-resolution imaging spectroradiometer (MODIS) ET estimates; (2) Calibrate and validate a modified Jarvis–Stewart (MJS) model to evaluate the influence of environmental forcing on lodgepole pine transpiration, and; (3) Demonstrate the utility and use of a Markov-Chain Monte Carlo (MCMC) approach via the Differential Evolution Adaptive Metropolis (DREAM) algorithm and a generalized likelihood (GL) function to parameterize the MJS model. This approach provides uncertainty estimates of the MJS model to allow interpretation of the model efficacy.

This study will assist future research that seeks to better understand the efficacy of vegetation removal on mountain meadows and similar environments while also considering the effects of changing climate on this land-management strategy. Additionally, to the authors' knowledge, sap-flow measurement has not been applied to a meadow-restoration research problem. The comparison of sap-flow-based lodgepole pine transpiration to MODIS ET estimates allows comments on the precision of this approach, broadening the reach of this work to sap-flow practitioners in general. Lastly, the application of the DREAM algorithm and GL function may assist future Jarvis-type transpiration (and stomatal conductance) modeling efforts.

2. Materials and Methods

2.1. Study Site

This research was done at Rock Creek Meadow (RCM), 40.329°, −121.088°, located near Chester, California, USA in the southern Cascade Range. RCM is on private forest land owned by Collins Pine Company (Figure 1). RCM is approximately 75 ha (185.3 ac), located at an elevation of 1525 m (5000 ft). The meadow underwent restoration by removal of lodgepole pine beginning in August 2020. The majority of the lodgepole pine was removed from RCM during fall 2020. Average lodgepole pine prior to removal had a basal area of 22.34 and 29.54 m^2/ha for the eastern and western meadow portions, respectively (Figure 1). A wildfire, the Dixie Fire (Plumas County, CA, USA), burned around and partially through RCM in August 2021.

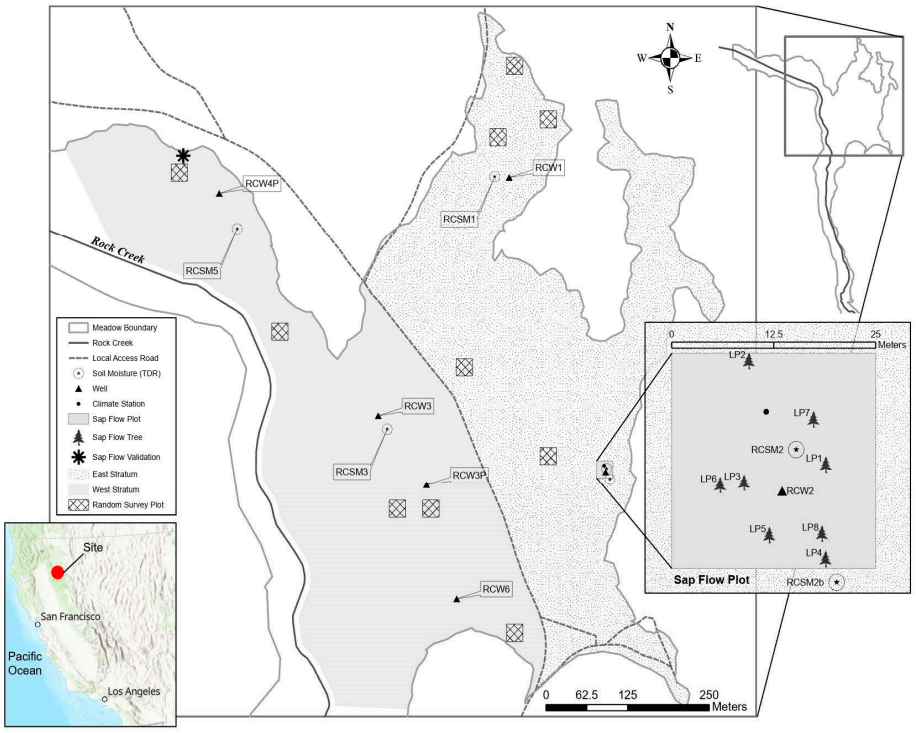

Figure 1. RCM near Chester, CA, including measurement locations. The sap-flow plot insert, displayed at a larger scale, shows the locations for the eight lodgepole pine (*Pinus contorta var. murryana* (Grev. & Balf.) Engelm.) (LP) instrumented for sap-flow measurement.

RCM climate is characterized by wet, cool winters and dry, warm summers. The average yearly precipitation from monthly normals is 873 mm (NOAAs ID USC00041700, 1981–2010). Most of the precipitation occurs during winter. RCM is generally classified as a dry meadow based on its observed hydrology and vegetation according to one meadow classification system [21]. Mesic meadow conditions exist in the western portion adjacent to Rock Creek, an intermittent watercourse.

RCM is in the Cascade Range and Modoc Plateau geomorphic provinces, with the Sierra Nevada geomorphic province just south. The geologic material is mapped as Pleistocene or Pliocene volcanic basalt rock. However, basaltic and rhyolitic rock has been observed at the meadow site. RCM consists of loamy textured soils. The western portion of the meadow (as separated by the road through the meadow, adjacent to Rock Creek, is mapped as Mountmed loam, 0 to 2 percent slopes. The eastern portion of the meadow is mapped as Inville very gravelly sandy loam, 0 to 5 percent slopes. Soil samples collected from the meadow coinciding with the Mountmed loam map unit at depths of less and greater than 20 cm textural classes (US Soil Taxonomy) of loam (31% sand, 44% silt, clay 25%) and silty clay loam (18% sand, 53% silt, 29% clay). Soil samples collected from the

meadow coinciding with the Inville very gravelly sandy loam map unit returned textural classes of sandy loam (50% sand, 37% silt, 13% clay) and loam (48% sand, 45% silt, 6% clay) at <20 cm and >20 cm depth, respectively.

2.2. Field Methods and Data

The field methods for this study include (1) measurement of lodgepole pine sap-flow, (2) measurement of meadow hydrometeorological conditions, linking lodgepole pine sap-flow with environmental variables, and (3) an interpretation of the spatial extent of lodgepole pine transpiration in a simple scaling approach using a plot tree survey. The sap-flow and hydrometeorological measurements served as calibration, input, and validation data for a modified Jarvis–Stewart model linking lodgepole pine sap-flow with environmental variables. Study methodology is discussed in further detail in [22].

2.2.1. Sap-Flow Measurements

Sap-flow was measured in lodgepole pine using three-probe configuration heat-pulse velocity sensors (East 30 Sensors, Pullman, WA, USA) following the design in [23]. The sensors were three 35 mm-long stainless-steel needles 6 mm apart. The middle needle consisted of an Evanohm heater (Carpenter Technology Corp., Philadelphia, PA, USA). Both the downstream and upstream needles featured three 10K precision thermistor sensors at distances of 5 mm, 17.5 mm, and 30 mm, respectively, from the probe shroud, allowing heat-velocity measurement at three radial depths.

The probes were installed in a 25 m-by-25 m plot in eastern RCM, hereafter referred to as the sap-flow plot (SFP) (Figure 1) in July 2019. Sap-flow instruments were removed from their respective trees in August 2020, corresponding with the beginning of restoration. The probes were moved to western RCM in May 2021 to provide validation data for the calibrated model (Figure 1 and Table 1). Eight lodgepole pines were selected for instrumentation within the SFP based on their diameter at breast height (DBH) (10–40 cm) and proximity to the data logger (Figure 1). Only six trees were instrumented due to sensor availability. The probes remained in the model validation trees until early July 2021.

Table 1. Sub-population (strata) and population (RCM) estimates of stem density, basal area, and sapwood (SW) basal area derived from the tree survey conducted at RCM via stratified random sampling. Parenthetical values represent one standard error. LP = lodgepole pine.

	E. Stratum	W. Stratum	RCM
Area (ha)	21.125	22.440	43.565
No. Random Plots	5	5	10
Stem Density (ha^{-1}) LP All DBH	1616.00 (513.25)	1641.60 (427.31)	1629.19 (291.43)
Stem Density (ha^{-1}) LP DBH > 10 cm	275.20 (32.16)	691.20 (201.65)	489.48 (92.58)
Stem Density (ha^{-1}) LP DBH 2.5–10 cm	1340.80 (495.57)	950.40 (293.92)	1139.71 (248.78)
Stem Density (ha^{-1}) Other tree species	112.00 (60.08)	115.20 (44.22)	113.65 (32.42)
Stem Density (ha^{-1}) All tree species	1728.00 (493.49)	1756.80 (411.68)	1742.84 (280.46)
Basal Area (m^2 ha^{-1}) LP	15.73 (1.21)	30.56 (6.27)	23.37 (2.89)
Basal Area (m^2 ha^{-1}) Other tree species	6.61 (3.11)	5.77 (2.38)	6.17 (1.70)
Basal Area (m^2 ha^{-1}) All tree species	22.34 (3.58)	36.33 (6.16)	29.54 (3.18)
SW Basal Area † (m^2 ha^{-1}) LP	10.77 (0.84)	20.90 (4.01)	15.99 (1.86)

† Estimated using regression equations for lodgepole pine sapwood and bark depth vs. DBH.

Heat-pulse velocity [L T^{-1}] was determined using the heat ratio method (HRM) based on [23,24]:

$$v_h = \frac{\beta}{x} \ln\left(\frac{\Delta T_d}{\Delta T_u}\right) \quad (1)$$

where v_h is the heat-pulse velocity (cm s^{-1}), β is the thermal diffusivity of green (fresh) sapwood (cm s^{-1}), x is the distance between the heater and either temperature probe (0.6 cm), and ΔT_d and ΔT_u are changes in temperature 60 s following heat pulse release at equidistant downstream and upstream points, respectively The accuracy of the heat-

pulse velocity calculation was improved by calculating site-specific thermal diffusivity for lodgepole pine sapwood and correcting for probe misalignment and tree wounding.

Thermal diffusivity was calculated for lodgepole pine [25]. A sapwood core was removed from each of the eight instrumented trees in the SFP in August 2020 using an increment borer (Haglöf, Sweden). Cores were also taken from the six instrumented trees at the validation site and two non-instrumented trees nearby in May 2021. The average thermal diffusivity from all samples (n = 16, 2.44 × 10^{-3} ± 2.3 × 10−4 cm^2/s) was used to calculate heat velocity for each tree.

The procedure [25] also informed the values of the water content of sapwood (ratio of water weight to dry wood weight), (m_c) and the basic density of sapwood (ρ_b) needed to calculate sap-velocity. Constant values of m_c = 1.00 ± 0.26 and ρ_b = 0.53 ± 0.11 g cm^{-3} were used.

Probe misalignment was corrected using the zero-flow approach [23]. The approach assumes that v_h= 0 cm hr^{-1} when there is no biophysical force driving transpiration. Zero-flow events were flagged when it was pre-dawn, soil moisture was close to saturation, and the vapor pressure deficit was close to zero, and they were used to correct for misaligned probes. Two instrumented trees between the SFP and model validation sites had severe probe misalignment at the 17.5 mm and 30 mm measurement depths. These data were abandoned in favor of the 5 mm depth data because of the uncertainty associated with correcting badly misaligned probes [23].

The published correction factors and equation were used to correct for wounding [23]. The wound correction was performed using the coefficients derived for a range of wound diameters corresponding to the −0.6, 0, and 0.6 cm probe configuration, where probes are 1.3 mm in diameter. Wounding corrections were only applied to the heat-velocity data collected in the SFP to use directly for lodgepole pine transpiration estimation. The wounding correction was unnecessary in the model validation deployment because the correction is a linear factor and is removed by the data normalization applied in our modeling approach. The average wound diameter was 2.4 ± 0.3 mm for the eight trees.

Corrected heat-pulse velocity (v_c) was converted to sap-velocity (v_s) [24] using the equation:

$$v_s = \frac{\rho_b}{\rho_s}\left(m_c + \frac{c_{dw}}{c_s}\right)v_c, \quad (2)$$

where ρ_b is the basic density of sapwood [M L^{-3}], ρ_s is the density of sap, assumed equal to water, m_c is water content of sapwood, c_s is the specific heat capacity of sap, assumed equal to water (4.186 kJ kg^{-1} K^{-1}), and c_{dw} is the specific heat capacity of oven-dry sapwood (kJ kg^{-1} K^{-1}). The normalized specific heat capacity of dry sapwood ($\frac{c_{dw}}{c_s}$) was calculated as a function of temperature [26–28]. Other works have assumed the normalized specific heat capacity as constant with a value of 0.33 (using c_{dw} = 1.380 kJ kg^{-1} K^{-1}) [29], but we adopt the former approach.

2.2.2. Meadow Hydrometeorological Conditions

Volumetric soil water content (VWC) and climate data were concurrently monitored with the sap-flow measurements at the study site. VWC was monitored at seven locations in RCM at depths ranging from 5 to 100 cm from the ground surface (Figure 1). VWC was computed from measured dielectric (relative) permittivity using the Topp equation [30]. A calibration check, comparing TDR probe values to laboratory gravimetric measurements, was performed in July 2020 using soil samples collected at 30 cm of depth in the vicinity of set-ups RCSM1, RCSM2b, and RCSM5. The two methods were found to be in good agreement.

A climate station (Onset) with sensors for air temperature, wind speed, wind direction, relative humidity, barometric pressure, and net shortwave solar radiation was installed in the SFP on 4 September, 2019 (Figure 1). Climate data prior to the installation of the station at RCM were taken from a station located in another research meadow 30 km west of RCM at similar elevation (1463 m) [10,12]. Daily precipitation data were collected from

the Chester, CA NOAA station (station ID USC00041700) part of the Global Historical Climatology Network daily database [31].

2.2.3. Tree Survey

A tree survey at RCM was done in July 2020. Measurements of lodgepole pine diameter at breast height (DBH), sapwood depth (D_s), and bark depth (D_b) were collected in 10 random plots (625 m^2) as part of a stratified random sampling design (STRS) (Table 1). The measurements were used to develop individual relationships of D_b and D_s versus lodgepole pine DBH using simple linear regression (Figure 2). The relationships were used to scale sap-velocity measurements in the SFP to trees in the random plots equally allocated between east and west strata of RCM (Figure 1). The stratification boundary was based on auxiliary information about site vegetation, soil moisture, and groundwater conditions. The STRS approach was chosen to ensure that the lodgepole pine forest at RCM was adequately sampled and potential decreases in the standard error associated with population parameter estimates.

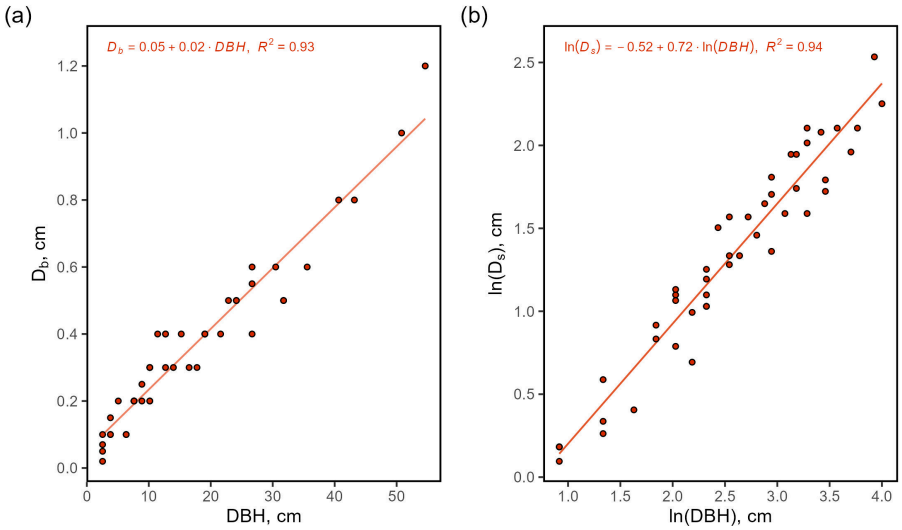

Figure 2. (**a**) Bark depth (D_b) versus diameter at breast height (DBH) and (**b**) sapwood depth (D_s) versus DBH in log–log space, both including simple linear regressions equation, R2, and line of best fit. Data (n = 47) in (**a**,**b**) are from cored trees sampled in the 10 random sample plots.

DBH was also measured for all lodgepole pine in the SFP and the three (3) 25 m by 25 m plots encompassing RCSM1, RCSM3, and RCSM5. The plots containing soil-moisture instruments were used for our extrapolation approach with the calibrated modified Jarvis–Stewart model.

2.3. Sap-Flow Modeling

We modeled sap-velocity from environmental variables to assess drivers of transpiration during one growing season. Soil moisture content was incorporated into the modelling to investigate soil water limitations. The calibrated model was used to estimate transpiration in select plots with soil-moisture sensors during the 2020 partial growing season (part of a dry year). This enabled exploration of the inclusion of spatially variable soil moisture in RCM-influenced sap-flow scaling in contrast to scaling informed only by the tree survey.

2.3.1. Model Data

The Modified Jarvis–Stewart (MJS) model was calibrated and validated using the average sap-velocity from instrumented lodgepole pine trees. We computed average sap-velocity from the measurement depth in each tree that was most frequently the largest (i.e., active depth) and averaging these values across trees [17].

Model calibration and validation were performed using normalized average sap-velocity ($\overline{v}_{s,n} = \overline{v}_s / \overline{v}_{s,max}$, dimensionless). Normalization to eliminate differences in magnitude between the average sap-velocity measurements at the SFP and validation locales during their respective monitored growing seasons was performed, thus facilitating an evaluation of model performance. We follow the normalization procedure by dividing the hourly average sap-velocity measurements ($\overline{v}_s$) by the average of the hourly 99.5th-percentile sap-velocity values from each instrumented tree's active depth ($\overline{v}_{s,max}$). The observation time series was reduced to an hourly interval [17]. Model forcing data consisted of hourly incoming solar radiation, vapor pressure deficit (VPD), air temperature, and VWC observations. Model calibration used normalized average sap-velocity and input data collected between 7 April and 17 August, 2020, while model validation used data collected between 1 May and 6 July 2021. 7 April was chosen as the start date for calibration modeling because this was the day the diurnal (maximum during the day and minimum at night) pattern indicative of transpiration returned to our sap-flow measurements. There would have been a longer period of data for the validation period. However, the sap-flow logger and probes were destroyed in the Dixie Fire in early August 2021. Both calibration and validation datasets excluded times where solar radiation was 0 W/m^2 (nighttime) or precipitation occurred, as done in other studies implementing an MJS model [17,32–34].

2.3.2. Modified Jarvis–Stewart Model

A modified Jarvis–Stewart (MJS) stomatal conductance model was used to predict normalized average sap-velocity from environmental variables [35,36]. The Jarvis–Stewart model modification adhered to the assumptions from [14]. Lodgepole pine transpiration (T), [L T^{-1}] is assumed to be proportional to the product of tree bulk canopy conductance (g_{bc}) [L $T^{-1}kPa^{-1}$], and the leaf-to-air vapor pressure deficit (D),

$$T = g_{bc} D \tag{3}$$

where D is VPD (kPa). Lodgepole pine transpiration is also assumed to be proportional to the normalized average sap-velocity (dimensionless),

$$T = \alpha \overline{v}_{s,n} \tag{4}$$

where α [L T^{-1}] is the product of maximum sap-velocity, sapwood cross-sectional area, and the profile of sap-velocity as a function of radius. Following the Jarvis–Stewart model, g_{bc} is modeled as maximum bulk canopy conductance (g_{bcmax}) reduced by environmental stress functions including f_R, f_D, f_{T_a}, and $f(\theta_v)$. Combining Equations (3) and (4) and substituting the result into Equation (5) yields

$$\overline{v}_{s,n} = \frac{g_{bcmax}}{\alpha} D * f_R * f_D * f_{T_a} * f(\theta_v) \tag{5}$$

The four stress functions in Equation (5) are empirically based and were selected from the literature. We chose functions used to predict conifer transpiration in an MJS model context that best fit our calibration dataset. Solar radiation stress was represented using Equation (6)

$$f_R = \frac{R}{R_{max}} \left(\frac{R_{max+k_R}}{R + k_R} \right) \tag{6}$$

where R is incoming solar radiation (W/m^2), k_R is a fitting parameter (dimensionless), and R_{max} is the maximum observed R during the model-calibration period (W/m^2) [33]. The VPD response was represented as

$$f_D = \frac{1}{1 + D/D_0} \tag{7}$$

where D is VPD (kPa) and D_0 is a parameter describing the sensitivity of sap-velocity to VPD (kPa) [17,37–39]. We use a function for air temperature:

$$f_{T_a} = e^{-k_a \frac{(T_a - T_0)^2}{T_a + T_0}} \quad (8)$$

where T_a is air temperature (°C), k_a is a fitting parameter (dimensionless), and T_0 is a parameter representing the optimal air temperature for sap-velocity after which sap-velocity begins to decline due to temperature stress (°C) [40]. Lastly, sap-velocity modulation by volumetric soil water content (VWC) was represented by

$$f(\theta_v) = \frac{1}{1 + e^{-k_s(\theta_v - \theta_0)}} \quad (9)$$

where k_s is a parameter describing the rate of decrease in sap-velocity under limiting VWC conditions (dimensionless), and θ_0 is the VWC value where sap-velocity decline is centered (dimensionless) [17,41].

Posterior distributions of the parameters contained in Equation (6) were identified using Markov Chain Monte Carlo (MCMC) simulation. The MCMC approach was executed using a version of the DiffeRential Evolution Adaptive Metropolis (DREAM) algorithm known as DREAM$_{(ZS)}$ [42]. The approach allowed identification of a maximum likelihood (ML) parameter set used to predict the normalized average sap-velocity for the validation site during the 2021 partial growing season. The MCMC approach and determined posterior distributions are available in [22].

2.4. Scaling of Sap-Flow and Model-Informed Transpiration Estimates

Lodgepole pine transpiration at RCM was estimated using a bottom-up sap-flow scaling approach [17,43–45]. The scaling required estimation of volumetric sap-flow, hereafter referred to as sap-flow, (Q) [$L^3\ T^{-1}$]. Sap-flow scaling was based on measurements taken in the SFP between 21 July 2019, and 16 August 2020. We also describe a scaling variation performed using the calibrated MJS model ML parameter estimates between 7 April 2020 and 16 August 2020.

2.4.1. Tree Sap-Flow

The tree sap-velocity measurements were used to estimate sap-flow, assuming a change in sap-velocity with increasing sapwood depth. The sap-velocity radial profile, sampled at multiple depths, was not well constrained in the inner portion of the sapwood approaching the heartwood. The probe sensor depth was 30 mm; all of the instrumented trees had sapwood that exceeded this depth [21]. Therefore, we estimate sap-flow using different assumptions for the sampled and non-sampled sapwood in the instrumented trees.

For the sapwood sampled, we estimated sap-flow using a weighted average approach [46]. Sap-flow for the sapwood not sampled was calculated with Equation (10) [17].

$$Q = 2\pi v_s \int_{r_{in}}^{r_{out}} r f_p(r) dr \quad (10)$$

where r is the radial position on the cross-section of the tree (not including bark), r_{in} (cm) is the radial position of the heartwood–sapwood boundary, r_{out} (cm) is the radial position of the innermost annulus bounding the sapwood not sampled by the probe, v_s is the sap-velocity provided by the innermost measurement point (cm h^{-1}), and $f_p(r)$ is a dimensionless linear function between 0 and 1 describing the radial profile of sap-velocity between the innermost sap-velocity measurement point and heartwood. The sap-velocity radial profile was approximated as in [17]. The profile is assumed to decline linearly with depth, based on previous research that sap-velocity is lower in the inner sapwood

compared to the outer sapwood in conifers [47–49]. We employ three simple variants of a sap-velocity profile:

$$f_{p,1}(r) = 1, f_{p,2}(r) = 1 + \frac{1}{2}\left(\frac{r - r_{out}}{r_{out} - r_{in}}\right), \text{ and } f_{p,3}(r) = 1 + \left(\frac{r - r_{out}}{r_{out} - r_{in}}\right), \quad (11)$$

where $f_{p,1}(r)$ retains constant sap-velocity across the sapwood, $f_{p,2}(r)$ decreases sap-velocity linearly to half of sap-velocity at the heartwood–sapwood boundary, and $f_{p,3}(r)$ decreases sap-velocity linearly to zero at the heartwood–sapwood boundary [17]. Sap flow for each instrumented tree was calculated as the sum of the estimate [46] and Equation (10). For measurements of tree DBH, sapwood depth, and bark depth used for calculations see [22].

2.4.2. Plot and Meadow Landscape Sap-Flow

Sap-velocity measurements made in the eight instrumented trees were extrapolated to the SFP and the 10 random plots part of the STRS. Plot sap-flow (Q_p, cm^3 h^{-1}) was estimated by summing individual tree sap-flow for all non-instrumented lodgepole pine (i) in a plot. Plot sap-flow was calculated three times for each plot using the same sap-velocity profiles provided by Equation (12) for $f_p(r)$:

$$Q_p = 2\pi\overline{v}_s \sum_{i=1}^{N} \int_{r_{in,i}}^{r_{out,i}} r f_p(r) dr \quad (12)$$

where $\overline{v}_s$ (cm h^{-1}) is average sap-velocity from the instrumented lodgepole pine in the SFP, $r_{in,i}$ is the radial position of the heartwood–sapwood boundary (cm), and $r_{out,i}$ is the radial position of the bark–sapwood boundary (cm). Plot transpiration (T) (mm h^{-1}) was calculated as a flux by dividing plot sap-flow by the plot area (625 m^2). Lastly, the calibrated MJS model was used to estimate transpiration in the plots containing soil moisture instruments RCSM2b (SFP), RCSM1, RCSM3, and RCSM5. Normalized average sap-velocity (dimensionless) was predicted with the ML parameter estimates [21] and used to estimate plot sap-flow:

$$Q_p = 2\pi\overline{v}_{s,max}\overline{v}_{s,n} \sum_{i=1}^{N} \int_{r_{in,i}}^{r_{out,i}} r f_p(r) dr \quad (13)$$

where $\overline{v}_{s,\max}$ (cm h^{-1}) is maximum $\overline{v}_s$ and $\overline{v}_{s,n}$ (dimensionless) is predicted average normalized sap-velocity for trees in a plot. Transpiration scaling informed by the calibrated MJS model was performed for the four plots between 7 April and 16 August, 2020 (2020 partial growing season). Volumetric soil water content input data for this period were provided by the respective soil moisture set-up in each plot, while the climate station in the SFP provided climate input data.

3. Results

3.1. Environmental Conditions and Sap-Velocity Measurements

The environmental conditions during SFP measurements are displayed (Figure 3). Average daily air temperature varied between −7.94 °C in December 2019 and 21.01 °C in August 2020 (Figure 3d). The maximum and minimum daily averages aligned with the maximum and minimum monthly temperature averages. The annual cycle of VPD followed temperature, peaking in August 2019 and July 2020 (Figure 3d). Maximum solar radiation was in late June in both years, corresponding with the summer solstice. The lowest daily solar radiation values were on days with high cloud cover, often corresponding with precipitation events (Figure 3b). Climate and energy conditions were similar between both growing seasons. A total of 1102 mm of precipitation fell during the 2019 WY overlapping with the beginning of SFP measurement, while 512 mm fell during the 2020 WY. Most

of the precipitation was snow, making the majority of reported yearly totals as snow–water equivalents.

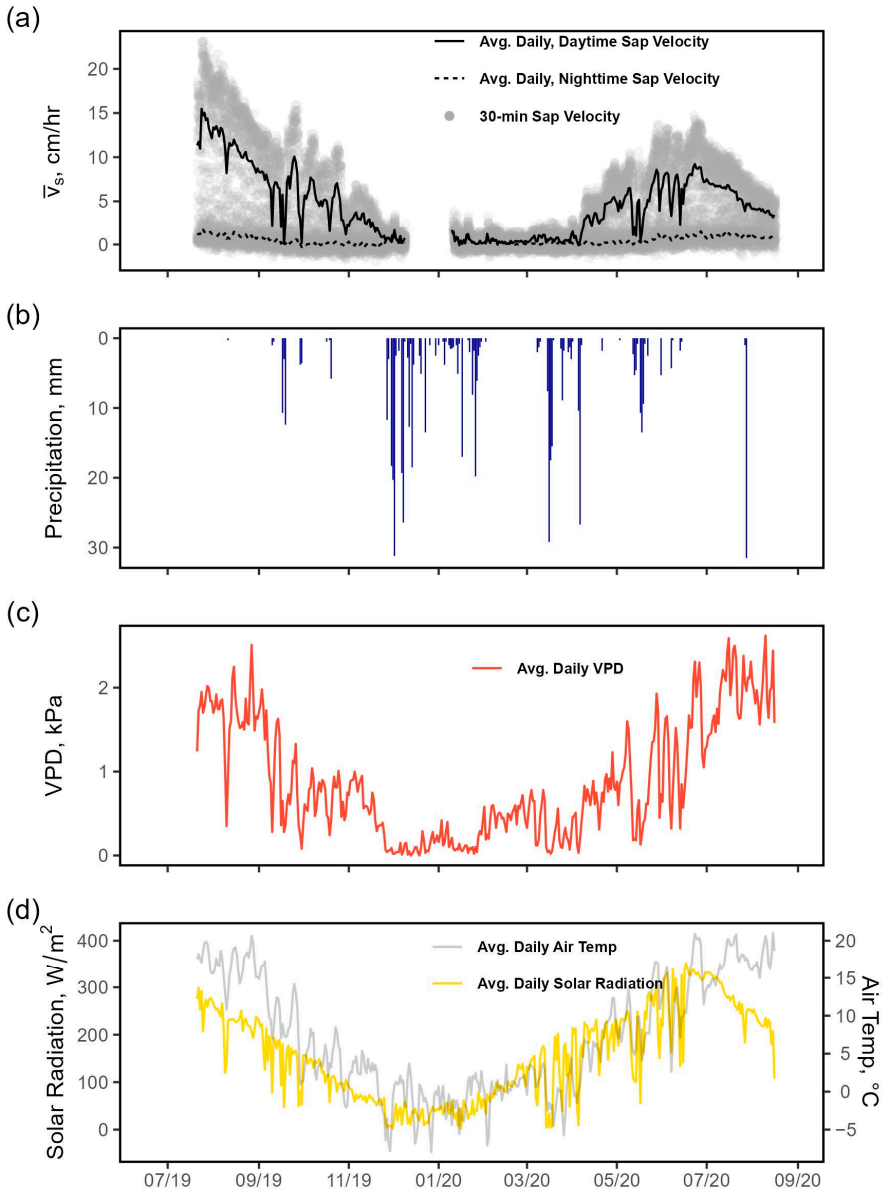

Figure 3. (**a**) 30 min average sap-velocity and daily average daytime and nighttime sap-velocity; (**b**) daily total precipitation; (**c**) average daily VPD; and (**d**) average daily incoming solar radiation and air temperature.

The average sap-velocity for lodgepole pine followed seasonal patterns throughout the monitoring period (Figure 3a). Sap-velocity followed a diurnal pattern with midday peaks at the beginning of the campaign in July and August 2019, coinciding with high daily VPD, solar radiation, and air temperatures.

The average daily sap-velocity was highest in the 2019 summer (11.54 $\pm$ 1.89 cm h^{-1}) compared to other seasons. The average daytime sap-velocity for the 2019 summer was greater than the 2020 summer velocity (6.05 $\pm$1.73 cm h^{-1}). From 1 April to 16 August 2020 (2020 partial growing season), the average daytime sap-velocity was 5.11 $\pm$ 2.15 cm h^{-1}.

3.2. MJS Model ML Parameter Estimates and Response to Environmental Variables

The maximum likelihood (ML) estimates provided well-defined functional dependencies to describe the relationships between normalized average sap-velocity and envi-

ronmental drivers. The non-limited functional dependencies (solid lines) representing the prediction of normalized average sap-velocity for a particular stress function, when all other stress functions are fixed at a value of 1, are shown (Figure 4). Additional functional dependencies (dotted and dashed lines) representing how the non-limited curves for each stress function are adjusted with changes in environmental drivers in the model. For example, the prediction of normalized average sap-velocity from the air temperature function responds to different values of VWC. The air temperature function would be adjusted further depending on values of incoming solar radiation and VPD. The resulting functional dependencies suggest varying degrees of sensitivity of sap-velocity to environmental drivers.

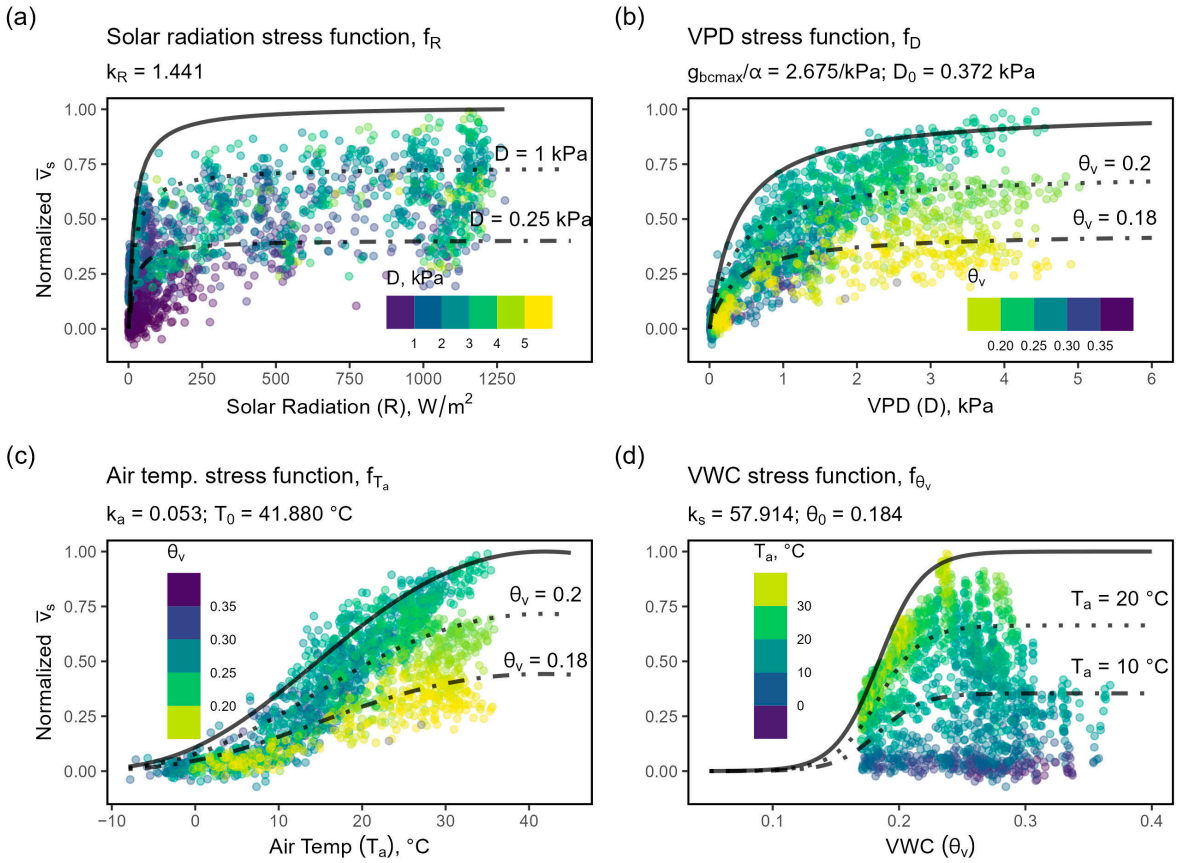

Figure 4. Hourly $\overline{v}_{s,n}$ response to environmental drivers for the calibration period: (**a**) $\overline{v}_{s,n}$ vs. solar radiation with different values of VPD; (**b**) $\overline{v}_{s,n}$ vs. VPD with different values of VWC; (**c**) $\overline{v}_{s,n}$ vs. air temperature with different values of VWC; and (**d**) $\overline{v}_{s,n}$ vs. VWC with different values of air temperature.

The response to incoming solar radiation by normalized average sap-velocity is fit by the shape parameter k_R, describing the curvature of the assumed asymptotic relationship between sap-velocity and solar radiation. The ML estimate of k_R is low, within its prior uniform distribution range. Accordingly, the solar radiation functional dependency shows saturation toward $\overline{v}_{s,n}$= 1 at approximately 100 W m^{-2} (Figure 4a). Normalized average sap-velocity rapidly increases at low values of solar radiation and fails to increase at high values of solar radiation.

The functional relationships of normalized average sap-velocity and VPD, air temperature, or VWC are tightly coupled to the observed data (Figure 4b,c). Average sap-velocity, as controlled by D_0 and $g_{bcmax/\alpha}$, gradually increased with VPD, plateauing at high values (Figure 4b,c). The plateauing effect at high VPD values is exaggerated when other environmental drivers are associated with non-limited sap-velocity (e.g., VWC > 0.35, Figure 4b). The non-limited VPD functional dependency does not reach $\overline{v}_{s,n} = 1$ over a realistic domain

of VPD values (Figure 4b). The air temperature functional dependency shows the greatest rate of normalized average sap-velocity increase between 0 and 25 °C, with maximum normalized average sap-velocity after approximately 30°C. The upper threshold, 41.88 °C, is represented by T_0, after which sap-velocity is assumed to decrease from temperature stress. The VWC functional dependency results in a decline of normalized average sap-velocity when soil moisture is at $\theta_0 = 0.184$. The VWC function indicates little sap-velocity limitation when the VWC is greater than 0.25 (Figure 4d). The k_s parameter controls the rate of decline in the function with decreasing VWC values, interpreted as limiting sap-velocity.

A qualitative point of comparison for the normalized average sap-velocity response between the calibration and validation periods is shown (Figure 5). Notably, the functional dependencies from the ML parameter estimates (calibration) for incoming solar radiation, VPD, and air temperature were similar in their coupling to observations from the validation period (Figure 5). We were unable to evaluate the validation performance for a full range of soil moisture conditions, interpreted as limiting by the calibration period, due to wildfire (Dixie Fire) destroying the sap-flow equipment in early August 2021.

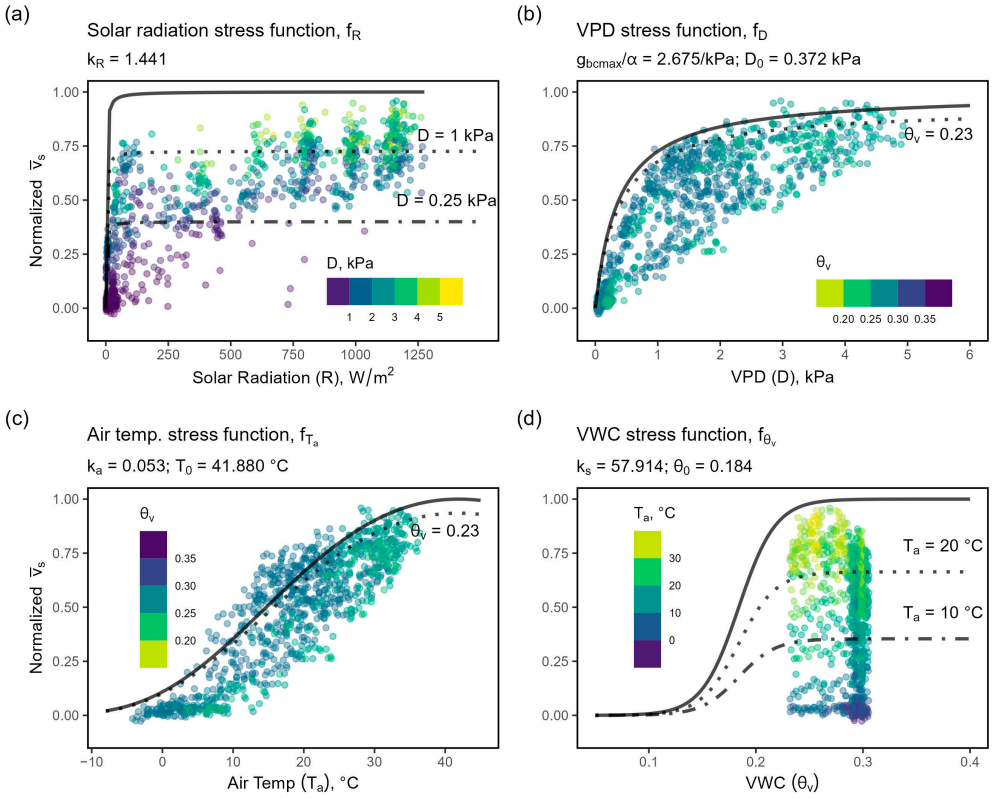

Figure 5. Hourly $\overline{v}_{s,n}$ response to environmental drivers for the validation period: (**a**) $\overline{v}_{s,n}$ vs. solar radiation with different values of VPD; (**b**) $\overline{v}_{s,n}$ vs. VPD with different values of VWC; (**c**) $\overline{v}_{s,n}$ vs. air temperature with different values of VWC; and (**d**) $\overline{v}_{s,n}$ vs. VWC with different values of air temperature.

3.3. MJS Model Performance

The variation in the observed data was better explained by the model during the calibration period (RMSE = 0.087) compared to the validation period (RMSE = 0.1233). The RMSE of 0.087 for calibration equates to an average sap-velocity of 1.25 cm h^{-1} after removing the normalization constant ($\overline{v}_{s,max}$ = 14.33 cm hr^{-1}). The ML parameter estimates had an average tendency to underpredict normalized average sap-velocity, with negative PBIAS for both periods (PBIAS = −6.579% for calibration and PBIAS = −2.873% for validation).

Additional model performance indicators are provided in Figure 6. There is a strong linear relationship between observed and predicted values for the calibration period, with a slope of linear regression close to 1 (Figure 6a). The linear fit for the validation is also strong (slope = 0.9), but there is a greater scatter around the simple linear regression (SLR) line, corresponding with the larger RMSE computed for this period relative to calibration (Figure 6b). The linear regressions coupled with the 1:1 line show the negative PBIAS for both periods. The SLR regression line intersects and dips below the 1:1 line at an approximate observed $\overline{v}_{s,n}$ value of 0.18 for the calibration period and 0.33 for validation, highlighting the tendency of the MJS model to underpredict high $\overline{v}_{s,n}$ values.

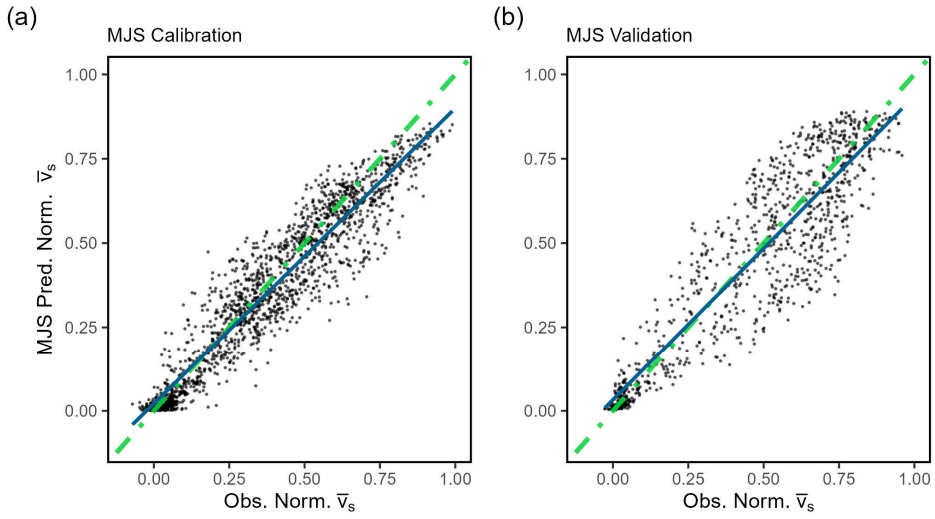

Figure 6. MJS predicted vs. observed normalized average sap-velocity for the (**a**) calibration period (y = 0.022 + 0.88x, R^2 = 0.89) and (**b**) validation period (y = 0.033 + 0.9x, R^2 = 0.89), including 1:1 line (dashed green) and SLR line (blue).

The parameter uncertainty bounds associated with model predictions for the calibration and validation periods are presented (Figure 6). The model generally underpredicted midday peaks. The inset graphs in Figure 6 emphasize that the parameter uncertainty bands frequently do not predict the measured midday observations.

The parameter uncertainty associated with model predictions for the calibration and validation periods is presented in Figure 7. Model underprediction was most common around midday peaks. The inset graphs in Figure 7 emphasize that the parameter uncertainty bands, let alone the ML parameter estimates, frequently fail to envelop midday observations.

Figure 8 shows a 95% total predictive uncertainty confidence interval for the calibration and validation periods, determined using the GL function error model parameter posterior distributions and the algorithm [50]. The predictive uncertainty bands envelop close to the theoretically expected 95% of total observations for the calibration period (94.5%).

The interval envelops a comparable 81.8% of total observations from the validation period. Parameter uncertainty is minimal relative to the total predictive uncertainty for both calibration and validation. Accordingly, almost all midday observations are captured in the total uncertainty band for both periods.

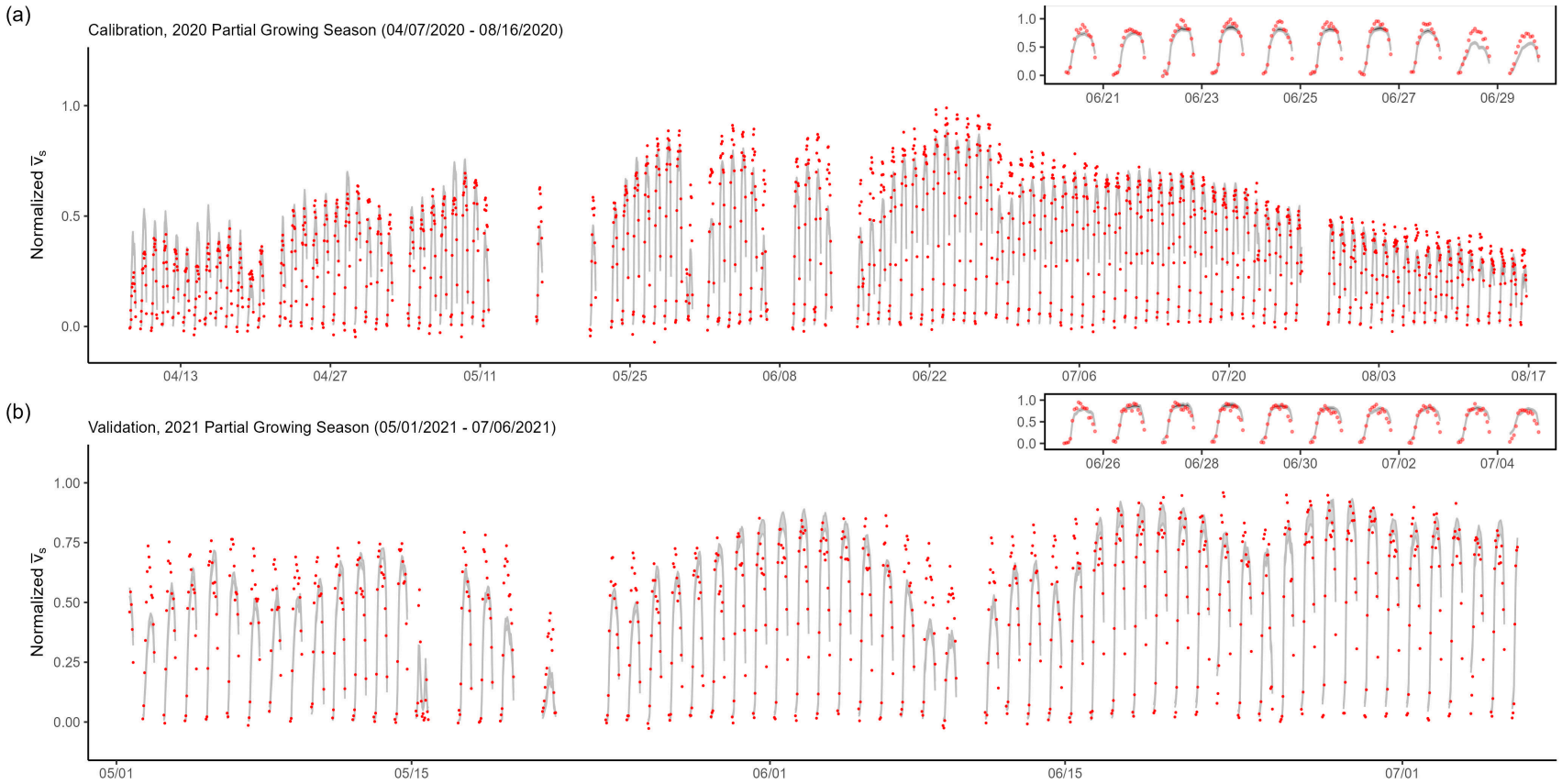

Figure 7. Ninety-five percent parameter uncertainty confidence interval and normalized average sap-velocity observations (red points) for (**a**) calibration and (**b**) validation periods. Gaps in the time series represent observation data that were removed from the analysis due to precipitation or it being nighttime. Insets show 10 days of sap-velocity observations, corresponding to 95% confidence parameter uncertainty interval for each period.

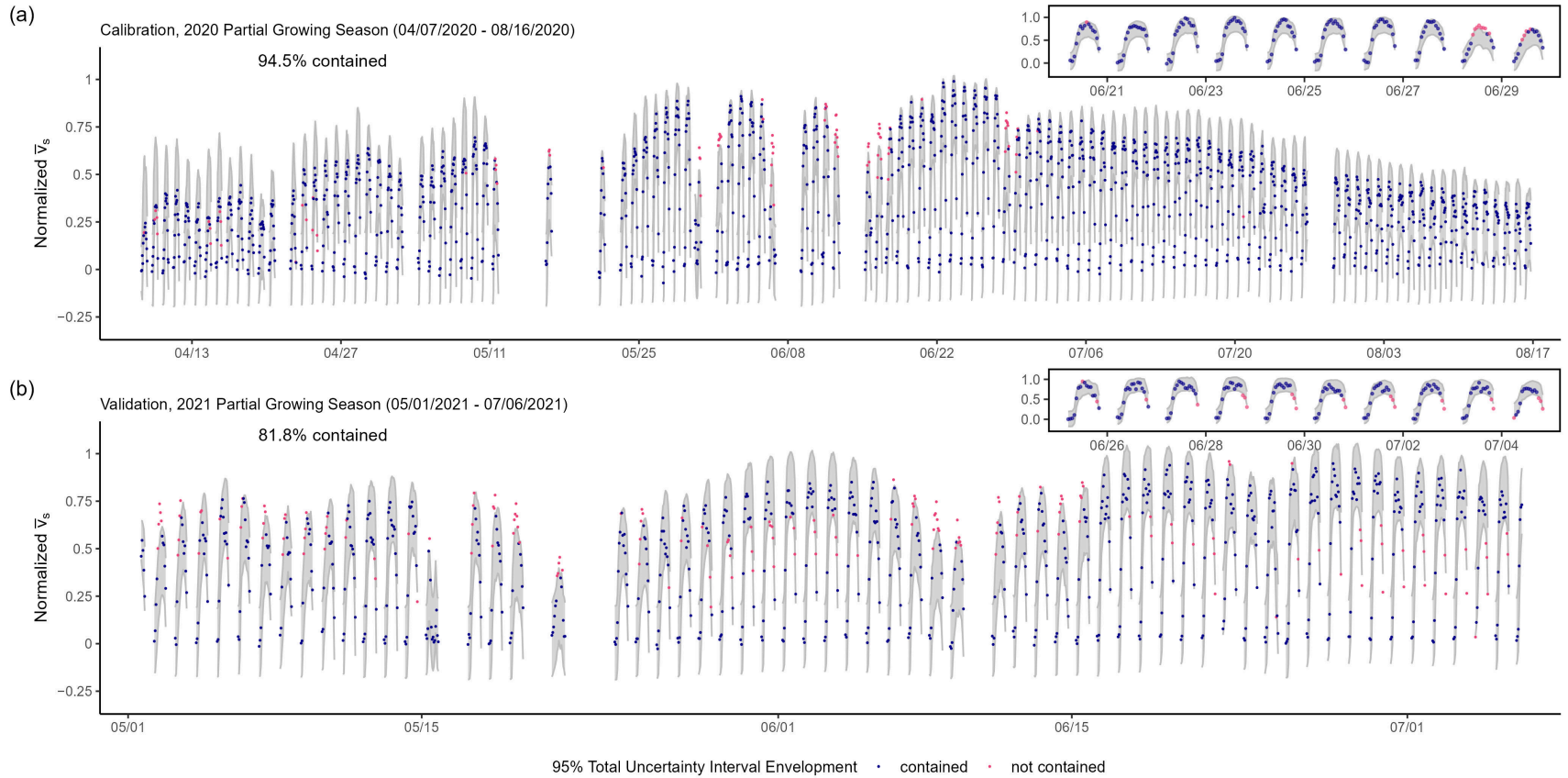

Figure 8. Ninety-five percent total predictive uncertainty confidence interval and normalized average sap-velocity observations (blue and red points) for (**a**) calibration and (**b**) periods. Insets show 10 days of sap-velocity observations, corresponding to 95% confidence parameter uncertainty interval for each period.

3.4. Simple Transpiration Estimates

Total transpiration and standard errors for RCM were calculated through the STRS design. The average total transpiration for RCM was estimated between 220.6± 25.3 mm and 393.4 ± 45.7 mm, given by $f_{p,3}(r)$ and $f_{p,1}(r)$, respectively, for the entire monitoring period (Table 2; Figure 9).

Table 2. Seasonal mean transpiration (T) total estimates by sap-velocity radial profile for east stratum, west stratum, and RCM. Second-row values for each season represent one standard error of the mean. GS = growing season.

Season	Total T, mm (East)			Total T, mm (West)			Total T, mm (RCM)		
	$f_{p,1}(r)$	$f_{p,2}(r)$	$f_{p,3}(r)$	$f_{p,1}(r)$	$f_{p,2}(r)$	$f_{p,3}(r)$	$f_{p,1}(r)$	$f_{p,2}(r)$	$f_{p,3}(r)$
Summer 2019 †	78.1	61.0	43.9	151.3	118.0	84.7	115.8	90.3	64.9
	6.1	4.8	3.5	29.0	22.5	16.1	13.4	10.4	7.4
Fall 2019	55.8	43.6	31.4	108.2	84.4	60.6	82.8	64.6	46.4
	4.4	3.5	2.5	20.8	16.1	11.5	9.6	7.5	5.3
Winter 2019 †	7.1	5.5	4.0	13.7	10.7	7.7	10.5	8.2	5.9
	0.6	0.4	0.3	2.6	2.1	1.5	1.2	1.0	0.7
Spring 2020	42.8	33.4	24.1	82.9	64.7	46.4	63.5	49.5	35.6
	3.4	2.6	1.9	15.9	12.4	8.8	7.4	5.7	4.1
Summer 2020 †	81.5	63.7	45.8	157.9	123.1	88.4	120.8	94.3	67.8
	6.4	5.0	3.7	30.3	23.5	16.8	14.0	10.9	7.8
Partial GS 2020 †	120.5	94.2	67.8	233.6	182.2	130.7	178.8	139.5	100.2
	9.4	7.4	5.5	44.8	34.8	24.8	20.7	16.1	11.5

† Transpiration estimate incomplete for season.

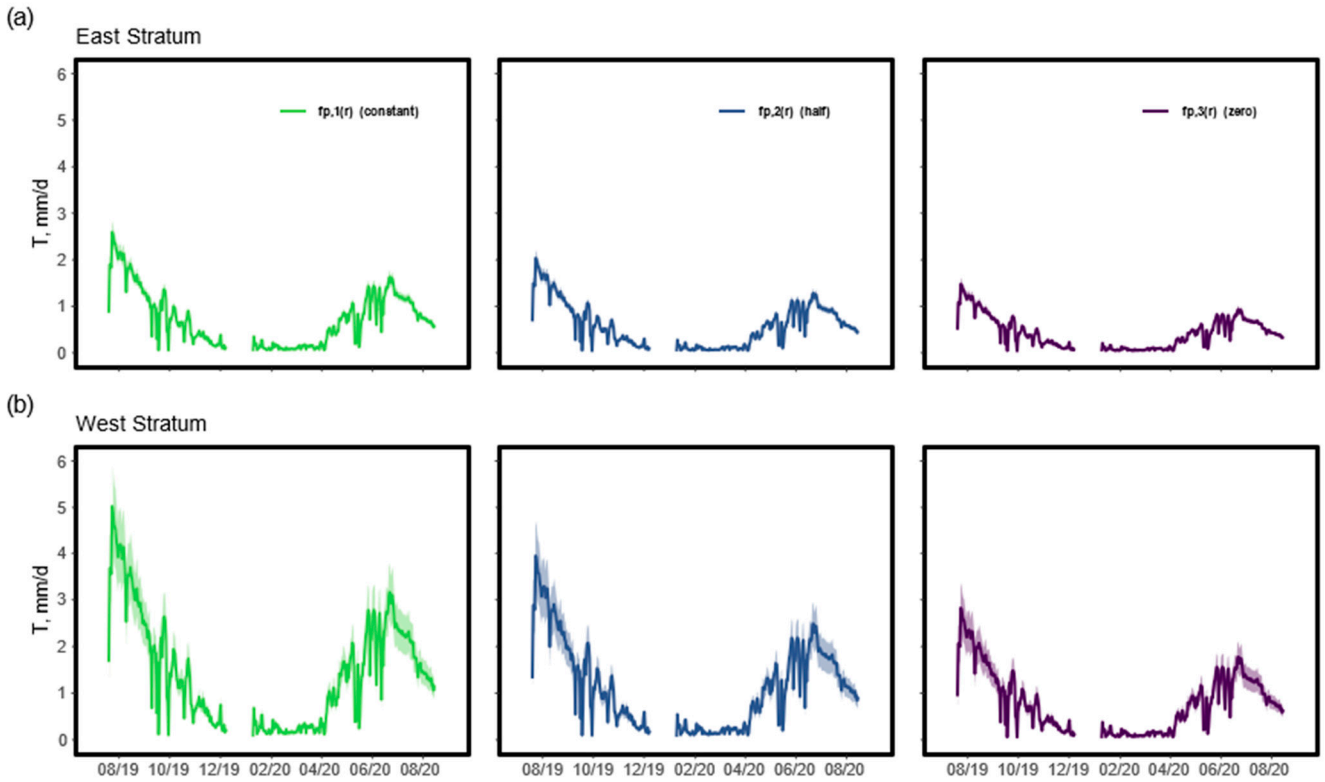

Figure 9. Daily average transpiration (T) estimated for the random plots in the (**a**) east stratum and (**b**) west stratum by sap-velocity radial profile. Ribbons represent ± 1 standard error of the daily mean.

Lodgepole pine transpiration estimates were compared to MODIS-derived evapotranspiration (MODIS ET) (MOD16A2GF product) 8-day composite estimates for the 2019 and

2020 calendar years via the AppEEARS application [51,52]. The timing of peak sap-flow predicted transpiration and MODIS ET was similar in the 2019 growing season (Figure 10). MODIS ET peaked from 12 July through 19. The highest 8-day transpiration from the 2019 growing season was 28 July through 4 August. This sum was similar to the composite provided for 20 July through 27, which summed 1 less day due to the SFP campaign beginning on 21 July 2019. Transpiration declines for the 2019 growing season began in early 21 August for both estimates. The timing of peak MODIS ET during the 2020 growing season was more dissimilar to peak lodgepole pine transpiration. Lodgepole pine transpiration peaked from 17 June through 24, while the largest MODIS ET composite was from 24 May through 31.

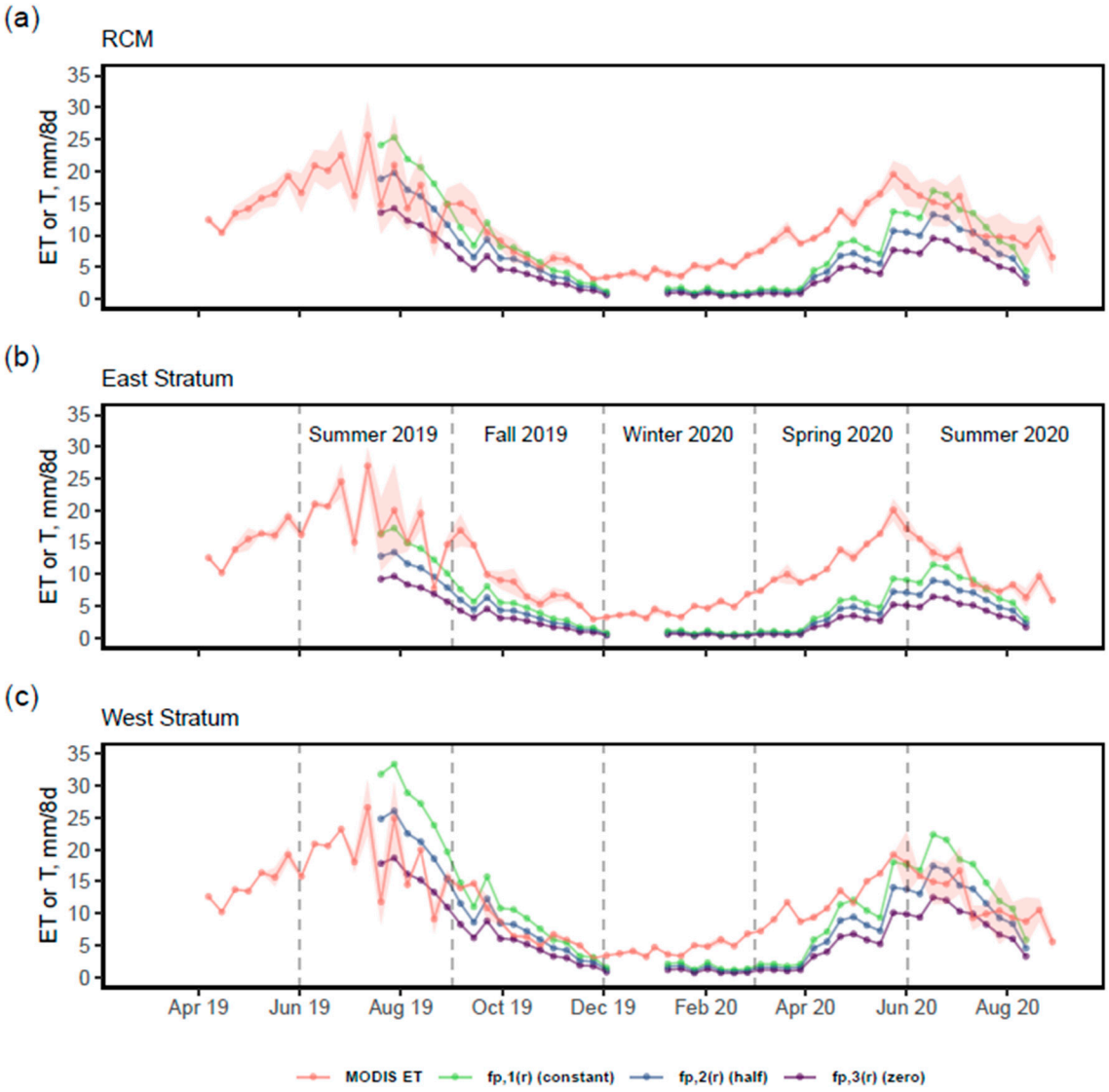

Figure 10. Time series of 8-day composite MODIS ET estimates compared with 8-day composite lodgepole pine transpiration (T) estimates by sap-velocity radial profile for (**a**) RCM, (**b**) east stratum, and (**c**) west stratum. Ribbons represent ±1 standard deviation of the MODIS ET 8-day composite, weighted mean.

The difference between the 8-day MODIS ET composites and the lodgepole pine transpiration estimates (residuals) were mostly positive values (Figure 11). The east stratum had the highest positive residuals. RCM and east and west stratums had positive residuals that gradually increased during winter 2020 into the spring before decreasing toward 0 mm in the summer. A similar trend was present between summer and fall in 2019. Large

negative residuals are observed for the west stratum in late July and early August 2019, especially for $f_{p,1}(r)$ and $f_{p,2}(r)$. Negative residuals are also seen for RCM and the east stratum in these months, albeit not as extreme.

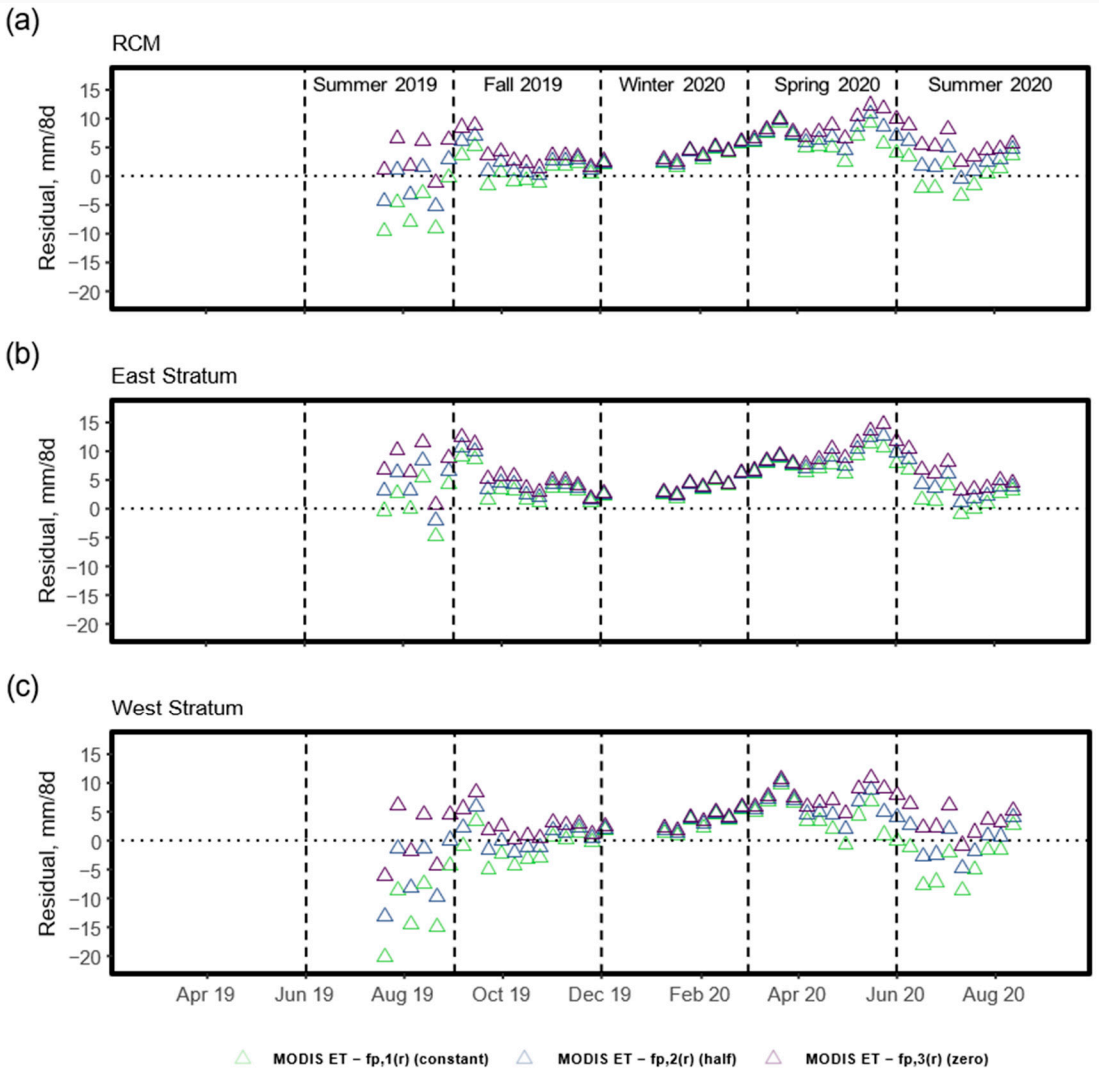

Figure 11. Time series of residuals between 8-day composite MODIS ET estimates and 8-day composite lodgepole pine transpiration (T) estimates by sap-velocity radial profile for (**a**) RCM, (**b**) east stratum, and (**c**) west stratum.

3.5. MJS-Informed Transpiration Estimates

The MJS model was used to estimate transpiration for the RCM plots containing soil-moisture measurements (Table 3, Figure 12). The transpiration estimates were slightly greater than MJS estimates for the SFP due to the model underpredicting observed sap-velocity. The MJS model does not consider nighttime transpiration.

Table 3. Comparison of lodgepole pine transpiration totals in soil moisture-containing plots informed by the calibrated MJS model and simple scaling for the period of 7 April through 16 August 2020.

	Total T, mm (MJS)			Total T, mm (Simple)		
Plot	$f_{p,1}(r)$	$f_{p,2}(r)$	$f_{p,3}(r)$	$f_{p,1}(r)$	$f_{p,2}(r)$	$f_{p,3}(r)$
SFP (RCSM2b)	65.2	56.7	48.1	69.3	59.9	50.6
RCSM1	58.3	45.0	31.7	90.0	69.5	48.9
RCSM3	70.9	55.5	40.2	85.6	67.2	48.5
RCSM5	320.3	248.1	175.9	303.9	235.4	167.0

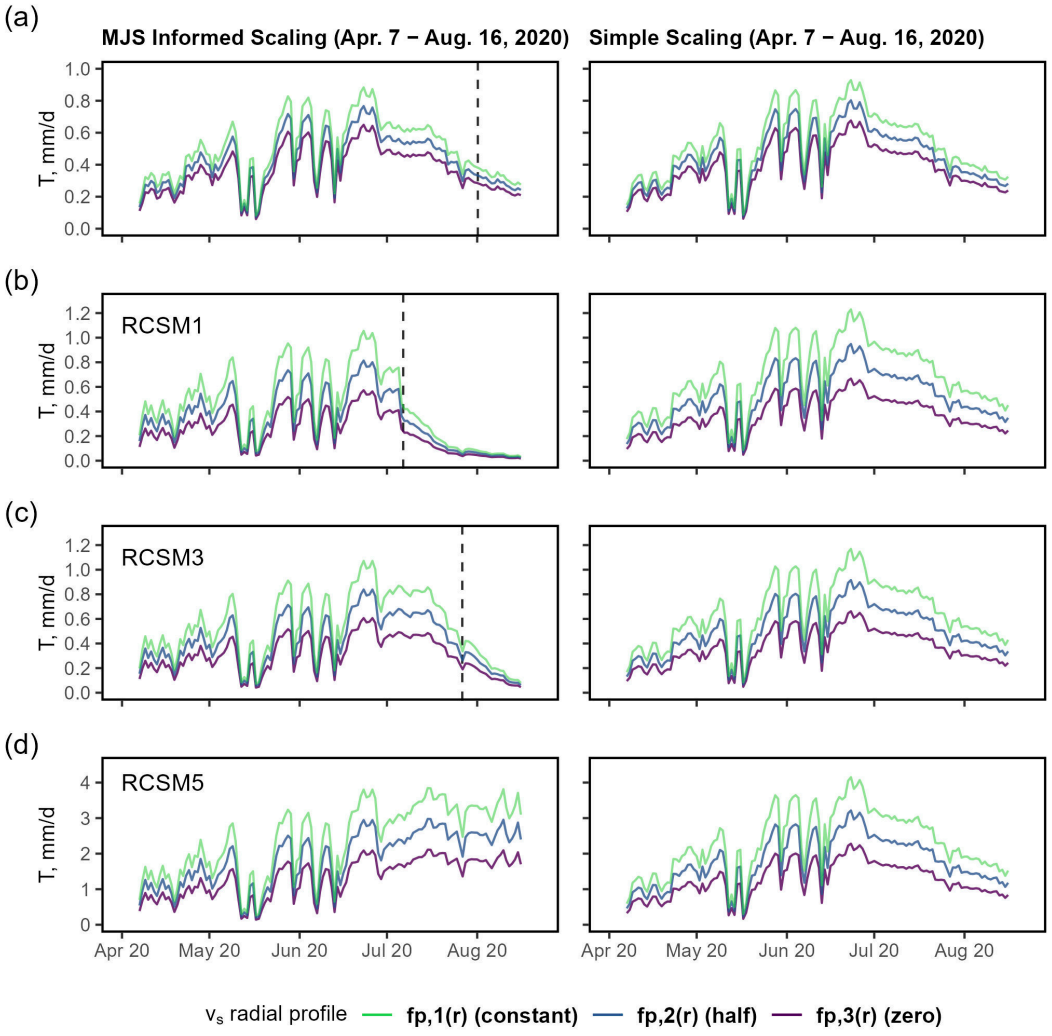

Figure 12. Comparison of daily transpiration (T) estimates informed by calibrated MJS model and simple scaling for soil moisture set-up containing plots: (**a**) SFP (RCSM2b), (**b**) RCSM1, (**c**) RCSM3, and (**d**) RCSM5. The vertical dashed lines mark when VWC dropped below 0.184 during the period shown. Note the differences in vertical scale used for (**a**–**d**).

The MJS transpiration estimates differed more noticeably from those produced by simple scaling in plots RCSM1, RCSM3, and RCSM5. RCSM1 featured the most extreme differences in estimated transpiration. RCSM1 VWC went below 18.4% (ML θ0 parameter estimate) on 6 July, 2020, and continued to diminish into the growing season, leading to low predictions of sap-velocity and low transpiration estimates (Figure 12b). VWC went below 18.4% in RCSM3 on 27 July, creating steadily declining transpiration estimates (Figure 12c). RCSM5 was the only plot to have transpiration estimates greater than the simple scaling.

4. Discussion

4.1. Assessment of Simple Lodgepole Pine Transpiration Estimates

As stated previously, one goal of this work was to estimate lodgepole pine transpiration in RCM for an approximately 1-year period. Sap-flow measurements were collected in the same eight trees in the SFP between July 2019 and August 2020. Many studies cite inter-tree variation in sap-flow measurements as a major source of transpiration spatial and temporal variation, with modulators including micro-meteorology, stand structure, topography, and soil moisture conditions [39,53–58]. The potential of soil moisture and sap-velocity spatial autocorrelation is of consideration at RCM because of the discrepancy in soil water, especially in the late growing seasons when we observed earlier soil drying in eastern RCM compared to western RCM. At the SFP scale, we observed differences in the lodgepole pine average sap-velocity measurements between the two partial growing seasons (Figure 3a). The inter-growing season variability in average sap-velocity is likely attributable to soil moisture differences between years due to differences in precipitation, as other climatic and energy conditions were similar (Figure 3). Similar observations have been noted for other conifer species during the growing season with antecedent dry and wet winters [59,60]. Ideally, sap-velocity would have been measured in multiple plots in both meadow sections per the recommendations of existing sap-flow scaling logic research [61,62].

The MODIS ET comparison allows for an assessment of the simple lodgepole pine transpiration estimates for RCM and the east and west strata part of the STRS. Overall, the comparison suggests that the lodgepole pine transpiration estimates are of a reasonable magnitude, especially for eastern RCM. The transpiration estimates for the three sap-velocity radial profiles for the eastern stratum were generally lower than their MODIS ET counterparts for the entirety of the campaign (Figures 10 and 11). This result is expected because the sap-flow derived estimate neglects transpiration from other vegetation in the meadow, as well as the soil and canopy evaporation considered by the MOD16A2 algorithm [63]. The residuals were closest to zero for the eastern stratum during fall 2019 and late summer 2020, which is likely explained by the dry soils and lack of wet canopy surface during these periods (Figure 11b). In contrast, larger positive residuals correspond with the winter and spring months when soil and canopy evaporation is expected to comprise a substantial amount of ET. Consideration of soil evaporation likely explains the discrepancy in the observed timing in peak MODIS ET and sap-flow-derived transpiration during the 2020 growing season.

Negative residuals were calculated for the western stratum (Figure 11c). The negative residuals occurred during late summer 2019, fall 2019, and summer 2020 and were especially pronounced for the $f_{p,1}(r)$ estimate. This disagreement might be due to inaccuracy in the lodgepole pine transpiration estimate for the western stratum, a consequence of its derivation from sap-flow measurements made in eastern RCM. However, the transpiration estimates computed from the $f_{p,2}(r)$ and $f_{p,3}(r)$ radial profiles featured fewer negative residuals compared to $f_{p,1}(r)$. Lodgepole pine transpiration would be expected to comprise a larger proportion of ET in western RCM relative to eastern RCM due to the high lodgepole pine stem density and sapwood area, coupled with higher VWC (Table 1). This emphasizes that the $f_{p,1}(r)$ radial profile likely overestimates lodgepole pine transpiration in assuming a constant sap-velocity across the sapwood radial profile. Past research has shown evidence that conifers, including lodgepole pine, generally exhibit a decrease in sap-velocity magnitude with sapwood depth [47–49].

Differences between estimated transpiration and MODIS ET may also be attributed to MOD16A2GF product pixel coarseness and/or limitations of the MOD16A2 algorithm for RCM. Figure 11 suggests the former, as the MODIS ET composites are similar among the east stratum, west stratum, and RCM. Notably, the MOD16A2 estimates are slightly higher for the eastern stratum versus the western stratum, whereas we would expect the opposite to be true. This similarity may be due to MOD16A2 pixel spatial distribution and size. The pixels overlapping RCM are not independent for the two strata and capture adjacent forested areas outside the meadow boundary. Furthermore, the findings of [64]

suggest that the MODIS ET estimate for our study site may be lower than the true ET, especially for the growing season months in the western stratum. In addition, [64] found that monthly flux tower measurements in the Southern Sierra Nevada (CA, USA) were consistently underestimated by the MOD16A2 ET product for wet and dry years at upper (2700 m) elevation sites dominated by conifer species, including lodgepole pine. Also, [64] attributed large underestimations of warm-season ET to the MOD16A2 algorithm imposing an over-excessive VPD limitation on canopy conductance. The algorithm accounts for water stress on transpiration using VPD [62].

4.2. Assessment of MJS Model-Informed Transpiration Estimates

The MJS-informed scaling and comparison to the simple scaling approach highlight some of the benefits and limitations of using the calibrated model to estimate lodgepole pine transpiration. The simple scaling transpiration estimates derived from the $f_{p,1}(r)$, $f_{p,2}(r)$, and $f_{p,3}(r)$ radial profiles in the SFP that were underestimated by 6.11%, 5.61%, and 4.92%, respectively, by the model (Table 3). Other studies have observed a similar underestimation of hourly MJS model-based transpiration estimates [32].

Soil-moisture conditions were spatially and temporally variable throughout RCM during the 2020 growing season. The benefit of including VWC in a scaling approach compared to the simple scaling is apparent for the RCSM5 plot estimate. RCSM5 showed ample soil moisture into the late growing season so that soil moisture conditions were perceived as unlimited to lodgepole pine transpiration by the model (Figure 12d). The MJS model validation for sap-velocity data in western RCM supports this, as observations of high sap-velocity were maintained with observations of high VWC (Figure 5d). Therefore, the simple scaling logic likely produces inaccurately low transpiration for the late-growing season in the RCSM5 plot.

In contrast to RCSM5, RCSM1 and RCSM3 recorded VWC values commensurate with the lodgepole pine transpiration soil moisture limitation perceived by the calibrated model during the growing season. This contributed to lower predicted transpiration in these plots compared to the simple scaling, especially after VWC dropped below 18.4% (Figure 12b,c). The rate of decline in predicted transpiration was especially steep after this threshold. This observation illuminates the poor constraints of the k_s parameter in the calibrated model; both RCSM1 and RCSM3 recorded VWC values lower than what was observed in the SFP during the calibration period. We would have higher confidence in the predicted transpiration in plots RCSM1 and RCSM3 had the model been calibrated using the full range of VWC observations in all soil moisture-monitored plots. Also, our model validation exercise was limited because we did not record any VWC values coincident with the sap-velocity decline observed during model calibration. This has a greater bearing on the model-derived transpiration estimates in RCSM3, as this plot was in western RCM. There is uncertainty, therefore, if the lodgepole pine in this plot would respond consistently with the SFP to declines in VWC.

Overall, these results emphasize the need to calibrate the model for a longer period and at multiple meadow locations. There are some model deficiencies that limit the model-informed scaling at RCM. Firstly, the approach requires knowledge about the average maximum sap-velocity for lodgepole pine. The model used the average of the 99.5th-percentile sap-velocity values from the instrumented SFP trees, but other studies using an MJS scheme also rely on an observed maximum sap-velocity or transpiration rate for a particular tree species [17,40]. Others allow this maximum to be parameterized in the model [31–34,36,65]. In the model-based scaling, it was assumed that the derived maximum average sap-velocity is spatially universal for RCM during the 2020 growing season. This is an unlikely assumption, especially for extrapolation to western RCM, which provided the soil moisture discrepancy in this meadow region. Secondly, the model used in this study is not able to simulate nocturnal sap-velocity, as is the case with most MJS models [40].

4.3. Sap-Velocity Response to Drivers during the Dry Growing Season

Like other studies on conifer sap-flow, fluctuations in solar radiation, VPD, and air temperature appear to modulate the diurnal variability in lodgepole pine average sap-velocity, while soil moisture regulates these relationships in the late growing season [17,18,39,66]. We note this study monitored and modeled using shallow soil moisture. Lodgepole pine reached near-maximum transpiration when VPD was above 3.5 kPa and the air temperature was greater than 30 °C when the 45 cm VWC exceeded a threshold of approximately 0.23. The effect of the declining VWC on the relationship between normalized average sap-velocity and each of the VPD and air temperature was apparent (Figure 4b–d).

Normalized average sap-velocity decline, in the 2020 growing season, corresponded with an approximate decrease in VWC from 0.23 to 0.17 between late June and mid-August. The soil moisture parameter, θ_0, prescribes that the sap-velocity decline is centered on a VWC value of 0.184. The range of VWC is coincident with sap-velocity decline, and the θ_0 parameter estimate is comparable to the results of other studies that assessed conifer sap-flow response to declining soil moisture. For example, another study showed declines in *Pinus taeda* stomatal conductance at a VWC threshold of 0.22 in clay loam soil [66]. A decline in *Pinus contorta* ssp. *latifolia* sap-flux density was found when soil moisture declined from 0.35 to 0.24 at 0–45 cm of depth in an inceptisol soil during the late growing season of a drought year [18]. We acknowledge that differences in soil properties between sites likely impart variation in tree water-use response to soil water conditions. The SFP in this study featured a sandy loam soil textural class, which typically has a field capacity between 0.16 and 0.22 and a wilting point of 0.073 VWC [67]. Our observations of sap-velocity decline and the θ_0 model parameter fall within these field capacity bounds, but this might be expected because conifers have been shown to be conservative with water use, especially in drought years [68]. The other soil moisture function parameter, k_s, describes the rate of sap-velocity decline under limiting VWC conditions. Because we did not have observations of VWC < 0.17 at the SFP, the decline-rate parameter for our site is not well constrained for VWCs less than this value.

4.4. Model Performance Using DREAM(zs) and the GL Function

Several studies have empirically parameterized an MJS model to predict conifer sap-velocity, sap-flux density, or transpiration. Some works have used an MCMC approach [17,32,40], while others have used optimization routines such as the genetic algorithm and quasi-Newton gradient-descent method [34,65]. The use of the DREAM$_{(ZS)}$ algorithm and the GL function in this study allowed for the avoidance of severe violations of residual autocorrelation, non-normality, and heteroscedasticity. It also allowed for a robust uncertainty assessment, which is useful when discussing model limitations and generalities. Uncertainty analysis and residual violations are typically not thoroughly addressed in empirical MJS parameterizations [69].

The strong performance of model fit for the validation period (RMSE = 0.1233) was somewhat surprising, as the validation data were different both spatially and temporally from the calibration data. Ignoring the magnitude of average sap-velocity, the response of normalized average sap-velocity to meteorological drivers at the validation site was similar to calibration (Figure 5a–c). High/maximum values of sap-velocity corresponded with comparable values of air temperature, VPD, and VWC to calibration. The response of sap-velocity to decreasing VWC into the late growing season is uncertain, but we might expect a different response due to the difference in soil properties between calibration and validation sites (e.g., sandy loam versus loam textural classes and differences in soil organic matter content). The shortened validation period also may have impacted the data normalization based on the average of the 99.5th-percentile sap-velocity values from each tree. It is possible that the validation period failed to capture maximum sap-velocity for the entire growing season, as data were not retrievable after July 6th. A lower normalization constant would result in artificially high normalized average sap-velocity values and likely poorer model performance. This might also explain the less negative PBIAS for the

validation compared to calibration. The model tended to under-predict observations of normalized average sap-velocity for both the calibration and validation periods, especially for mid-day observations, corresponding with daily peaks (Figures 6 and 7). This concurs with other studies that attribute underestimation to model structural deficiencies [32,40]. The failure of MJS models to simulate the full range of sap-flow observations is due to the inability of the environmental stress functions to equal 1 at the same time [40]. One structural deficiency in our fitted model was the VPD stress function that did not reach the maximum normalized average sap-velocity over the observed domain of VPD values (Figure 4b).

Lastly, the parameter and total predictive uncertainty confidence intervals suggest the benefit of including an uncertainty analysis in an MJS model. Parameter uncertainty was small relative to total predictive uncertainty, suggesting that consideration of parameter uncertainty alone in our model was insufficient (Figures 7 and 8). MJS models have many uncertainties stemming primarily from a basic understanding of the relationship between environmental stressors and the tree physiology controlling water use. There is also incomplete knowledge of the spatial and temporal variability of the environmental input data and tree sap-flow response. The total uncertainty assessment is an attempt to account for such uncertainties and to combat the simplifications made by the model. The total uncertainty intervals for the calibration and validation periods seem reasonable, as they enveloped close to the theoretically expected 95% of total observations (Figure 7). The total uncertainty intervals captured most midday observations for both periods that were systematically underestimated by our model formulation.

5. Conclusions

The transpiration estimates in this study were based on a sap-flow monitoring campaign on a single plot of lodgepole pine in eastern RCM (SFP) where a sample of eight (8) trees was instrumented for an approximately 1-year period. The data were used with an STRS design of lodgepole pine sapwood depth in a simple, bottom-up sap-flow scaling approach to estimate transpiration for the meadow. The MODIS ET product comparison suggests the magnitude and timing of the estimated transpiration for each meadow partition in the STRS are reasonable, especially for the eastern stratum. However, the accuracy of this approach would likely improve by instrumenting lodgepole pine in the western stratum where soil water content was higher than in the eastern stratum. The agreement between MODIS ET and the transpiration estimates in the eastern stratum suggests the potential usefulness of using a small sample of trees for estimates of meadow transpiration.

The comparison of the calibrated MJS model informed transpiration scaling to simple scaling transpiration estimates suggests the model-based approach incorporating soil water content has potential for application in a montane meadow site water balance. It is recommended that the model be calibrated over a sufficient period and/or multiple locales within a study site.

Our MJS model and assessment of sap-velocity response to environmental drivers suggests that future warmer and drier growing seasons in this region may present occurrences of limited lodgepole pine water consumption, especially in the late growing season. This study was limited in a few aspects that prohibited rigorous exploration of certain hydrologic and climatic characteristics that may influence lodgepole pine transpiration in montane meadows within the context of a changing climate. The analysis in our study did not allow an assessment of the relative effects of environmental drivers on predicted sap-flow over the course of the growing season. A sensitivity coefficient analysis would be useful in assessing the effects of climatic variables on tree water use in the early growing season when soil moisture is non-limiting, which is relevant to anticipated shifts in energy inputs with climate change. Second, no formal analysis was done to assess late-growing-season rainfall effects on lodgepole pine transpiration due to the lack of precipitation events in the late 2020 growing season.

The performance results of the MJS model parameterized using the DREAM$_{(ZS)}$ algorithm and the GL function in this study show potential for future use with MJS models. The total predictive uncertainty analysis methodology in this modeling approach considers the prevalent structural deficiencies of MJS models.

Author Contributions: Conceptualization, S.M. and C.S.; methodology, S.M., C.S. and B.M.; formal analysis, S.M.; investigation, S.M. and C.S.; resources, C.S.; data curation, S.M. and C.S.; writing—original draft preparation, S.M.; writing, review, and editing, S.M., C.S. and B.M.; visualization, S.M.; supervision, C.S.; project administration, C.S.; funding acquisition, C.S. All authors have read and agreed to the published version of the manuscript.

Funding: This research was funded by the Sierra Institute for Community and the Environment, through a Cal Fire California Climate Investments (CCI) Forest Health Grant, South Lassen Watersheds Group Collaborative Landscape Restoration Project (Agreement 8GG18615). The cost of restoration forestry work and this research has been supported by funding from the Sierra Institute for Community and the Environment, through a Cal Fire California Climate Investments (CCI) Forest Health Grant, South Lassen Watersheds Group Collaborative Landscape Restoration Project (Agreement 8GG18615). Additional funding came from the California State Universities Agriculture Research Institute grant numbers ARI-03-020, ARI-03-026, ARI-23-02-101, and USDA-NIFA-McIntire-Stennis grant numbers CALY-1302 and 24-054.

Data Availability Statement: The data presented in this study are available on request from the corresponding authors.

Conflicts of Interest: The authors declare no conflicts of interest. The funders had no role in the design of the study; in the collection, analyses, or interpretation of data; in the writing of the manuscript; or in the decision to publish the results.

References

1. Viers, J.H.; Purdy, S.E.; Peek, R.A.; Fryjoff-Hung, A.; Santos, N.R.; Katz, J.V.; Emmons, J.D.; Dolan, D.V.; Yarnell, S.M. *Montane Meadows in The Sierra Nevada: Changing Hydroclimatic Conditions and Concepts for Vulnerability Assessment*; Technical Report CWS-2013-01; University of California Davis: Davis, CA, USA, 2013.
2. Stillwater Sciences. *A Guide for Restoring Functionality to Mountain Meadows of the Sierra Nevada*; Technical Memorandum 2012, Prepared for American Rivers; American Rivers: Nevada City, CA, USA; Berkeley, CA, USA, 2012.
3. Ratliff, R.D. *Meadows in the Sierra Nevada of California: State of Knowledge*; Technical Report 1985, PSW-84; USDA Forest Service, Pacific Southwest Forest and Range Experiment Station: Berkeley, CA, USA, 1985.
4. Dailey, M.M. Meadow Classification in the Willamette National Forest and Conifer Encroachment Patterns in the Chucksney-Grasshopper Meadow Complex, Western Cascade Range, Oregon. Master's Thesis, Oregon State University, Corvallis, OR, USA, 2007.
5. Takaoka, S.; Swanson, F.J. Change in extent of meadows and shrub fields in the central western Cascade Range, Oregon. *Prof. Geogr.* **2008**, *60*, 527–540. [CrossRef]
6. Taylor, A.H. Forest expansion and climate change in the mountain hemlock (*Tsuga mertensiana*) zone, Lassen Volcanic National Park, California, USA. *Arct. Alp. Res.* **1995**, *27*, 207–216. [CrossRef]
7. Vale, T.R. Tree invasion of montane meadows in Oregon. *Am. Midl. Nat.* **1981**, *105*, 61–69. [CrossRef]
8. Lang, N.L.; Halpern, C.B. The soil seed bank of a montane meadow: Consequences of conifer encroachment and implications for restoration. *Botany* **2007**, *85*, 557–569. [CrossRef]
9. Swanson, F.J.; Halpern, C.B.; Cissel, J.H. *Restoration of Dry, Montane Meadows through Prescribed Fire, Vegetation and Fuels Management: A Program of Research and Adaptive Management in Western Oregon*; Project 01C-3-3-10; Joint Fire Science Program: Boise, ID, USA, 2019.
10. Surfleet, C.; Sanford, T.; Van Oosbree, G.; Jasbinsek, J. Hydrologic response of meadow restoration the first year following removal of encroached conifers. *Water* **2019**, *11*, 428. [CrossRef]
11. Fie, N. Hydrologic Response from Conifer Removal and Upslope Forest Harvest from an Encroached Montane Meadow. Master's Thesis, California Polytechnic State University, San Luis Obispo, CA, USA, 2018.
12. Surfleet, C.; Fie, N.; Jasbinsek, J. Hydrologic response of a montane meadow from conifer removal and upslope forest thinning. *Water* **2020**, *12*, 293. [CrossRef]
13. Mitsch, W.J.; Gosselink, J.G. The value of wetlands: Importance of scale and landscape setting. *Ecol. Econ.* **2000**, *35*, 25–33. [CrossRef]

14. Hammersmark, C.T.; Rains, M.C.; Mount, J.F. Quantifying the hydrological effects of stream restoration in a montane meadow, northern California, USA. *River Res. Appl.* **2008**, *24*, 735–753. [CrossRef]
15. Loheide, S.P., II; Gorelick, S.M. A local-scale, high-resolution evapo- transpiration mapping algorithm (ETMA) with hydroecological applications at riparian meadow restoration sites. *Remote Sens. Environ.* **2005**, *98*, 182–200. [CrossRef]
16. Cooper, A.E.; Kirchner, J.W.; Wolf, S.; Lombardozzi, D.L.; Sullivan, B.W.; Tyler, S.W.; Harpold, A.A. Snowmelt causes different limitations on transpiration in a Sierra Nevada conifer forest. *Agric. For. Meteorol.* **2020**, *291*, 108089. [CrossRef]
17. Link, P.; Simonin, K.; Maness, H.; Oshun, J.; Dawson, T.; Fung, I. Species differences in the seasonality of evergreen tree transpiration in a Mediterranean climate: Analysis of multiyear, half- hourly sap flow observations. *Water Resour. Res.* **2014**, *50*, 1869–1894. [CrossRef]
18. Pataki, D.E.; Oren, R.; Smith, W.K. Sap flux of co-occurring species in a western subalpine forest during seasonal soil drought. *Ecology* **2000**, *81*, 2557–2566. [CrossRef]
19. Albano, C.M.; McClure, M.L.; Gross, S.E.; Kitlasten, W.; Soulard, C.E.; Morton, C.; Huntington, J. Spatial patterns of meadow sensitivities to interannual climate variability in the Sierra Nevada. *Ecohydrology* **2019**, *12*, e2128. [CrossRef]
20. Hauptfeld, R.; Kershner, J.; Feifel, K. Sierra Nevada Ecosystem Vulnerability Assessment Technical Synthesis: Wet Meadows. In *A Climate Change Vulnerability Assessment for Focal Resources of the Sierra Nevada*; Version 1.0; Kershner, J., Ed.; EcoAdapt: Bainbridge Island, WA, USA, 2014.
21. Weixelman, D.A.; Hill, B.; Cooper, D.; Berlow, E.; Viers, J.; Purdy, S.; Merrill, A.; Gross, S. *A Field Key to Meadow Hydrogeomorphic Types for the Sierra Nevada and Southern Cascade Ranges in California*; Technical Report R5-TP-034; USDA Forest Service Pacific Southwest Region: Vallejo, CA, USA, 2014.
22. Marks, S.J. Estimating and Modeling Transpiration of a Mountain Meadow Encroached by Conifers Using Sap Flow Measurements. Master's Thesis, California Polytechnic State University, San Luis Obispo, CA, USA, 2021.
23. Burgess, S.S.; Adams, M.A.; Turner, N.C.; Beverly, C.R.; Ong, C.K.; Khan, A.A.; Bleby, T.M. An improved heat pulse method to measure low and reverse rates of sap flow in woody plants. *Tree Physiol.* **2001**, *21*, 589–598. [CrossRef]
24. Marshall, D. Measurement of sap flow in conifers by heat transport. *Plant Physiol.* **1958**, *33*, 385. [CrossRef]
25. Vandegehuchte, M.W.; Steppe, K. Improving sap flux density measurements by correctly determining thermal diffusivity, differentiating between bound and unbound water. *Tree Physiol.* **2012**, *32*, 930–942. [CrossRef]
26. Dunlap, F. *The Specific Heat of Wood*; Technical Report USDA Forest Service Bulletin 110; USDA: Washington, DC, USA, 1912.
27. Steppe, K.; De Pauw, D.J.; Doody, T.M.; Teskey, R.O. A comparison of sap flux density using thermal dissipation, heat pulse velocity and heat field deformation methods. *Agric. For. Meteorol.* **2010**, *150*, 1046–1056. [CrossRef]
28. Swanson, R.; Whitfield, D. A numerical analysis of heat pulse velocity theory and practice. *J. Exp. Bot.* **1981**, *32*, 221–239. [CrossRef]
29. Edwards, W.; Warwick, N. Transpiration from a kiwifruit vine as estimated by the heat pulse technique and the Penman-Monteith equation. *N. Z. J. Agric. Res.* **1984**, *27*, 537–543. [CrossRef]
30. Topp, G.C.; Davis, J.; Annan, A.P. Electromagnetic determination of soil water content: Measurements in coaxial transmission lines. *Water Resour. Res.* **1980**, *16*, 574–582. [CrossRef]
31. Menne, M.J.; Durre, I.; Vose, R.S.; Gleason, B.E.; Houston, T.G. An overview of the global historical climatology network-daily database. *J. Atmos. Ocean. Technol.* **2012**, *29*, 897–910. [CrossRef]
32. Wang, H.; Guan, H.; Simmons, C.T. Modeling the environmental controls on tree water use at different temporal scales. *Agric. For. Meteorol.* **2016**, *225*, 24–35. [CrossRef]
33. Whitley, R.; Medlyn, B.; Zeppel, M.; Macinnis-Ng, C.; Eamus, D. Comparing the Penman–Monteith equation and a modified Jarvis–Stewart model with an artificial neural network to estimate stand-scale transpiration and canopy conductance. *J. Hydrol.* **2009**, *373*, 256–266. [CrossRef]
34. Whitley, R.; Taylor, D.; Macinnis-Ng, C.; Zeppel, M.; Yunusa, I.; O'Grady, A.; Froend, R.; Medlyn, B.; Eamus, D. Developing an empirical model of canopy water flux describing the common response of transpiration to solar radiation and VPD across five contrasting woodlands and forests. *Hydrol. Process.* **2013**, *27*, 1133–1146. [CrossRef]
35. Jarvis, P. The interpretation of the variations in leaf water potential and stomatal conductance found in canopies in the field. *Philos. Trans. R. Soc. Lond. B Biol. Sci.* **1976**, *273*, 593–610. [CrossRef]
36. Stewart, J. Modelling surface conductance of pine forest. *Agric. For. Meteorol.* **1998**, *43*, 19–35. [CrossRef]
37. Dang, Q.L.; Margolis, H.A.; Coyea, M.R.; Sy, M.; Collatz, G.J. Regulation of branch-level gas exchange of boreal trees: Roles of shoot water potential and vapor pressure difference. *Tree Physiol.* **1997**, *17*, 521–535. [CrossRef]
38. Lohammar, T.; Larsson, S.; Linder, S.; Falk, S. FAST: Simulation models of gaseous exchange in Scots pine. *Ecol. Bull.* **1980**, *32*, 505–523.
39. Looker, N.; Martin, J.; Hoylman, Z.; Jencso, K.; Hu, J. Diurnal and seasonal coupling of conifer sap flow and vapour pressure deficit across topoclimatic gradients in a subalpine catchment. *Ecohydrology* **2018**, *11*, e1994. [CrossRef]
40. Wang, H.; Guan, H.; Liu, N.; Soulsby, C.; Tetzlaff, D.; Zhang, X. Im- proving the Jarvis-type model with modified temperature and radiation functions for sap flow simulations. *J. Hydrol.* **2020**, *587*, 124981. [CrossRef]
41. Feddes, R.A.; Kowalik, P.; Kolinska-Malinka, K.; Zaradny, H. Simulation of field water uptake by plants using a soil water dependent root extraction function. *J. Hydrol.* **1976**, *31*, 13–26. [CrossRef]

42. Laloy, E.; Vrugt, J.A. High-dimensional posterior exploration of hydrologic models using multiple-try DREAM (ZS) and high-performance computing. *Water Resour. Res.* **2012**, *48*. [CrossRef]
43. Ford, C.R.; Hubbard, R.M.; Kloeppel, B.D.; Vose, J.M. A comparison of sap flux-based evapotranspiration estimates with catchment- scale water balance. *Agric. For. Meteorol.* **2007**, *145*, 176–185. [CrossRef]
44. Jung, E.Y.; Otieno, D.; Lee, B.; Lim, J.H.; Kang, S.; Schmidt, M.; Tenhunen, J. Up-scaling to stand transpiration of an Asian temperate mixed- deciduous forest from single tree sapflow measurements. *Plant Ecol.* **2011**, *212*, 383–395. [CrossRef]
45. Solum, J.; Malama, B. Estimating canopy-scale evapotranspiration from localized sap flow measurements. *Water* **2022**, *14*, 1812. [CrossRef]
46. Hatton, T.; Catchpole, E.; Vertessy, R. Integration of sapflow velocity to estimate plant water use. *Tree Physiol.* **1990**, *6*, 201–209. [CrossRef]
47. Berdanier, A.B.; Miniat, C.F.; Clark, J.S. Predictive models for radial sap flux variation in coniferous, diffuse-porous and ring-porous temperate trees. *Tree Physiol.* **2016**, *36*, 932–941. [CrossRef]
48. Ford, C.R.; McGuire, M.A.; Mitchell, R.J.; Teskey, R.O. Assessing variation in the radial profile of sap flux density in Pinus species and its effect on daily water use. *Tree Physiol.* **2004**, *24*, 241–249. [CrossRef]
49. Mark, W.R.; Crews, D.L. Heat-pulse velocity and bordered pit condition in living Engelmann spruce and lodgepole pine trees. *For. Sci.* **1973**, *19*, 291–296.
50. Schoups, G.; Vrugt, J.A. A formal likelihood function for parameter and predictive inference of hydrologic models with correlated, heteroscedastic, and non-Gaussian errors. *Water Resour. Res.* **2010**, *46*. [CrossRef]
51. Appears Team. Application for Extracting and Exploring Analysis Ready Samples (AppEEARS). Available online: https://lpdaacsvc.cr.usgs.gov/appeears (accessed on 11 June 2021).
52. Running, S.W.; Mu, Q.; Zhao, M.; Moreno, A. MOD16A2GF MODIS/Terra Net Evapotranspiration Gap-Filled 8-Day L4 Global 500 m SIN Grid V006. 2019. Available online: https://lpdaac.usgs.gov/products/mod16a2gfv061/ (accessed on 11 June 2021).
53. Adelman, J.D.; Ewers, B.E.; Mackay, D.S. Use of temporal patterns in vapor pressure deficit to explain spatial autocorrelation dynamics in tree transpiration. *Tree Physiol.* **2008**, *28*, 647–658. [CrossRef]
54. Berry, Z.C.; Looker, N.; Holwerda, F.; Gómez Aguilar, L.R.; Ortiz Colin, P.; González Martínez, T.; Asbjornsen, H. Why size matters: The interactive influences of tree diameter distribution and sap flow parameters on upscaled transpiration. *Tree Physiol.* **2017**, *38*, 263–275. [CrossRef]
55. Loranty, M.M.; Mackay, D.S.; Ewers, B.E.; Adelman, J.D.; Kruger, E.L. Environmental drivers of spatial variation in whole-tree transpiration in an aspen-dominated upland-to-wetland forest gradient. *Water Resour. Res.* **2008**, *44*. [CrossRef]
56. Kumagai, T.; Aoki, S.; Nagasawa, H.; Mabuchi, T.; Kubota, K.; Inoue, S.; Utsumi, Y.; Otsuki, K. Effects of tree-to-tree and radial variations on sap flow estimates of transpiration in Japanese cedar. *Agric. For. Meteorol.* **2005**, *135*, 110–116. [CrossRef]
57. Tromp-van Meerveld, H.; McDonnell, J. On the interrelations between topography, soil depth, soil moisture, transpiration rates and species distribution at the hillslope scale. *Adv. Water Resour.* **2006**, *29*, 293–310. [CrossRef]
58. Moore, G.W.; Bond, B.J.; Jones, J.A.; Phillips, N.; Meinzer, F.C. Structural and compositional controls on transpiration in 40-and 450-year-old riparian forests in Western Oregon, USA. *Tree Physiol.* **2004**, *24*, 481–491. [CrossRef]
59. Brito, P.; Lorenzo, J.R.; Gonzalez-Rodriguez, A.M.; Morales, D.; Wieser, G.; Jimenez, M.S. Canopy transpiration of a semi arid Pinus canariensis forest at a treeline ecotone in two hydrologically contrasting years. *Agric. For. Meteorol.* **2015**, *201*, 120–127. [CrossRef]
60. Liu, X.; Biondi, F. Transpiration drivers of high-elevation five-needle pines (Pinus longaeva and Pinus flexilis) in sky-island ecosystems of the North American Great Basin. *Sci. Total Environ.* **2020**, *739*, 139861. [CrossRef]
61. Kume, T.; Tsuruta, K.; Komatsu, H.; Kumagai, T.; Higashi, N.; Shinohara, Y.; Otsuki, K. Effects of sample size on sap flux- based stand-scale transpiration estimates. *Tree Physiol.* **2010**, *30*, 129–138. [CrossRef]
62. Mackay, D.S.; Ewers, B.E.; Loranty, M.M.; Kruger, E.L. On the representativeness of plot size and location for scaling transpiration from trees to a stand. *J. Geophys. Res. Biogeosci.* **2010**, *115*, G02016. [CrossRef]
63. Running, S.W.; Mu, Q.; Zhao, M.; Moreno, A. *User's Guide MODIS Global Terrestrial Evapotranspiration (ET) Product (MOD16A2/A3 and Year-End Gap-Filled MOD16A2GF/A3GF) NASA Earth Observing System MODIS Land Algorithm (For Collection 6)*, 2.2 ed.; National Aeronautics and Space Administration: Washington, DC, USA, 2019.
64. Jepsen, S.M.; Harmon, T.C.; Guan, B. Analyzing the suitability of remotely sensed ET for calibrating a watershed model of a Mediterranean montane forest. *Remote Sens.* **2021**, *13*, 1258. [CrossRef]
65. Guyot, A.; Fan, J.; Oestergaard, K.T.; Whitley, R.; Gibbes, B.; Arsac, M.; Lockington, D.A. Soil-water content characterization in a modified Jarvis-Stewart model: A case study of a conifer forest on a shallow unconfined aquifer. *J. Hydrol.* **2017**, *544*, 242–253. [CrossRef]
66. Oren, R.; Ewers, B.E.; Todd, P.; Phillips, N.; Katul, G. Water balance delineates the soil layer in which moisture affects canopy conductance. *Ecol. Appl.* **1998**, *8*, 990–1002. [CrossRef]
67. Dunne, T.; Leopold, L.B. *Water in Environmental Planning*, 15th ed.; Freeman and Company Publishers: New York, NY, USA, 1998.

68. Royce, E.B.; Barbour, M.G. Mediterranean climate effects. I. Conifer water use across a Sierra Nevada ecotone. *Am. J. Bot.* **2001**, *88*, 911–918. [CrossRef]
69. Ford, C.R.; Goranson, C.E.; Mitchell, R.J.; Will, R.E.; Teskey, R.O. Modeling canopy transpiration using time series analysis: A case study illus- trating the effect of soil moisture deficit on Pinus taeda. *Agricultural and For. Meteorol.* **2005**, *130*, 163–175. [CrossRef]